INTERNSHIP REPORT

Estimating Future Costs and Carbon Footprints of PEMEC and SOEC Manufacturing

Zhichuan Ma

Supervised by
Pr. François Maréchal
Yi Zhao

Industrial Processes and Energy
Systems Engineering (IPESE) Laboratory
Ecole Polytechnique Fédérale de Lausanne

Autumn 2023

August 24, 2023

Abstract

The net-zero emission target necessitates a significantly expanded deployment of clean technologies compared to their current utilization. Precisely estimating the future potential of these technologies requires a thorough understanding of their cost and carbon footprint evolution. This study bridges the gap by integrating life cycle assessment (LCA) and cost estimation methodologies, resulting in a comprehensive bottom-up model that simultaneously evaluates the cost and carbon footprint, with particular attention to the scaling effect. This model is then applied to scrutinize the manufacturing processes of Proton Exchange Membrane Electrolysis Cells (PEMEC) and Solid Oxide Electrolysis Cells (SOEC). The assessment incorporates a detailed manufacturing process description and equipment inventory. It is found as manufacturing capacity increases, both the cost and carbon footprint decrease. Notably, at a low manufacturing capacity of 1MW/year, SOEC exhibits higher costs and a greater carbon footprint compared to PEMEC, with values of $900/MW and 110,000 kg/MW, respectively. However, SOEC's advantage lies in its superior scaling performance, attributed to more cost-effective and environmentally friendly raw material inputs. These results are leveraged to forecast future costs and carbon footprints of PEMEC and SOEC, offering valuable insights for further decarbonization of green hydrogen production.

Key words: Learning effect, Life cycle assessment, clean hydrogen, cost evolution, carbon reduction

Acknowledgements

I would like to thank various people for their help and contribution to this challenging and interesting project

I would like to offer a special thanks to Yi Zhao for his constant guidance and constructive critiques. He always took the time to give his feedback and thoughts towards the advancement of the project, and I am extremely grateful for that.

I would also like to thank Professor François Maréchal for his precious academic support.

Table of Contents

List of Figures

List of Tables

1 Introduction

1.1 Background

In the pursuit of achieving net-zero emissions, a transformation of the global energy system from fossil fuels to sustainable sources is crucial. This requires a substantial increase in the deployment of renewable technologies such as photovoltaics, wind power, and clean hydrogen production. According to the International Energy Agency (IEA), industrial hydrogen demand is projected to rise by 44% by 2030, with low-carbon hydrogen becoming increasingly important (expected to reach 21 million tonnes by 2030)[1]. While these clean technologies are currently in the early stages and face challenges like high costs and complex manufacturing, ongoing technological development and scaling up are expected to significantly reduce their costs and carbon footprints in the future.

Learning effect

The cost reduction of green technologies is closely associated with what is known as the learning effect. Initially introduced to describe the phenomenon of price reduction in relation to the global shipment of a particular technology, the learning effect has been a well-established concept for a long time. One of the most famous examples is the observation of the price reduction of photovoltaic panels. As shown in Figure 1, the price of PV modules decreased from almost 100 \$/W in 1976 to less than 1 \$/W in 2013 with the cumulative capacity development.

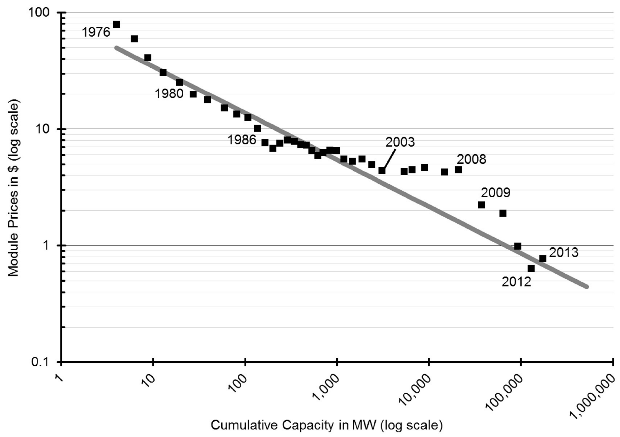

Figure 1: Learning curve of the solar PV module [2]

Equation 1 and 2 present the learning effect in mathematical form, where C_Q is the marginal cost of producing Q-th unit, C_1 is the cost of the first unit, β is an exponential and m refers to the learning rate [3]. An exponential correlation is found between the unit cost and the global cumulative production.

$$C_Q = C_1 Q^{\beta} \tag{1}$$

$$\beta = log(m)/log(2) \tag{2}$$

The learning effect is attributed to both low-level mechanisms such as reductions in material consumption and high-level mechanisms including the advancement of manufacturing, learning-by-doing (LBD) and scaling effect. Among them, the scaling effect is a major drive and reflects the decrease in manufacturing costs of products due to mass production. In other words, the cost per product declines steadily as the annual production volume increases when the size of products is fixed.

A bottom-up cost model

To explore the theories and underlying factors influencing the learning effect, a comprehensive bottom-up cost estimation model was developed by Lu [4] in 2022 within the Industrial Process and Energy Systems Engineering (IPESE) lab at EPFL. This model underwent validation through comparison with public databases and specific literature sources. It was employed to assess the costs associated with Proton Exchange Membrane Electrolyzer Cells (PEMEC) and Solid Oxide Electrolyzer Cells (SOEC) from multiple perspectives, including material costs and capital expenditures. The study found that, in scenarios where production volumes are relatively small, costs tended to decrease rapidly with increasing capacity, often following an exponential correlation. Within a factory throughput range of 500 MW/year to 10,000 MW/year, ongoing cost reductions were predominantly driven by enhanced utilization of equipment, labor, and facilities. Additionally, as plants scaled up further, costs tended to stabilize, approaching minimum levels determined by material costs. Notably, it was observed that at equivalent production capacities, PEMEC exhibited higher costs due to its utilization of noble metals. The study also elucidated six principles of Economies of Scale (EoS) with statistical evidence. By integrating this cost model with the concept of the learning curve and incorporating different parameters, the model shows potential for application in green hydrogen price forecasting and across various industries.

Life cycle assessment (LCA)

Life Cycle Assessment (LCA) is a widely employed method for evaluating environmental impacts behind various clean technologies, encompassing factors such as global warming potential (GWP), ozone depletion, particulate matter, etc. LCA methods typically involve intricate tracking of material and energy flows leaving and entering the environment. By assigning values to each of these flows using detailed information, it becomes possible to quantify the life cycle impact.

The popularity of LCA has grown since 1990, in tandem with increased environmental awareness [5]. However, LCA faced criticism during its early development due to high expectations. Over the years, there has been substantial progress and refinement in LCA standards and practices. In 2008, Jørgensen et al. [6] conducted a comprehensive LCA technology review. Since then, LCA's applications have expanded into various areas, including waste management, technology assessment, energy sector decision-making, and product system improvement. LCA's data-handling capabilities across a product's life cycle enable assessments of complex production and consumption systems[7].

1.2 Research gap

Two research gaps are identified in this study. First, cost can be considered as an additional dimension within the scope of LCA. Combining cost analysis with LCA could enhance the accuracy of cost analysis outcomes. Simultaneously, it could broaden our comprehension of the technology itself.

In addition, the application of the learning effect, typically employed to analyze cost evolution, can also be extended to the study of carbon footprint evolution. Surprisingly, this aspect is often overlooked in most LCA studies. It is suggested that the learning effect, originating from extensive production and encompassing contributions from manufacturing processes, could also play a role in carbon footprint reduction.

Building upon the cost model developed in the preceding year [4], this study extends its scope to encompass a more comprehensive bottom-up cost and Life Cycle Assessment (LCA) model. The report follows a structured approach. It begins by elucidating the methodology governing the life cycle assessment and cost estimation processes. Subsequently, our model is meticulously applied to a case study focusing on the manufacturing of Proton Exchange Membrane Electrolysis Cells (PEMEC) and Solid Oxide Electrolysis Cells (SOEC), offering an in-depth exposition of the equipment and processes involved. The ensuing discussion segment delves comprehensively into the costs and carbon footprint profiles associated with various manufacturing throughput scenarios. Building upon our analyses, we employ the results to project the anticipated cost evolution of PEM and SOEC into the future, providing valuable insights into potential trajectories. Concluding the report, we briefly present the cost of hydrogen production derived from PEM and SOEC technologies. This study integrates methodological rigor, exhaustive case analysis, and forward-looking projections to deliver a comprehensive assessment of the cost and environmental implications of PEMEC and SOEC manufacturing.

2 Methodology

One of the preliminary prerequisites in the formulation of a comprehensive cost and environmental impacts model is the establishment of boundaries. The comprehensive manufacturing process could be dissected into three phases: construction, production, and end-of-life (EOL) treatment. Antecedent to the culmination of final product realization, meticulous contemplation must be accorded to the construction of infrastructure and equipment, due to their consequential role in costs and environmental impacts. Hence, both the plants and the equipment are metaphorically postulated as tubular conduits, comprising a continuum of material and energetic constituents. The manufacturing trajectory unfolds within these conduits, wherein disparate material fluxes and energy flows converge. Within these conduits, these fluxes undergo a series of transformative reactions, producing the final products, together with some other ancillary by-products. Furthermore, it is noteworthy that these products may serve as inputs for subsequent phases. After long-term use, the plants and equipment will inevitably transition into the terminal phase of their life cycle, the end-of-life stage. During this phase, extra energy is input to undertake waste treatment and recycling endeavors. The general descriptive schema is as the following.

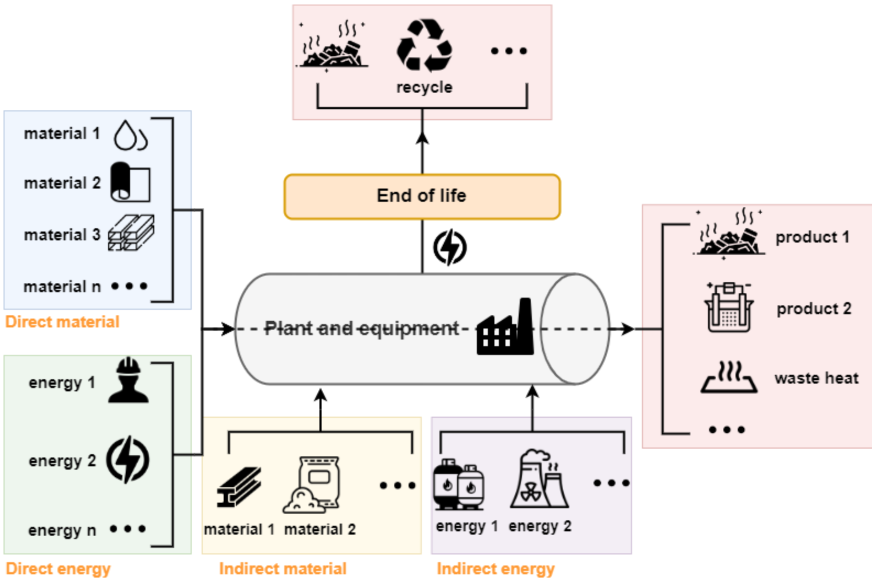

Figure 2: general methodology map

Derived from the aforementioned boundary, the envisaged approach for the computation of the ultimate product's cost and environmental impact is proposed. The overcoming formula is presented herein:

$$C_{unit} = \sum_{i=1}^{n} k_i m_i C_{i,material} + \sum_{i=1}^{q} k_i E_i C_{i,energy} \tag{3}$$

$$e_{unit} = \sum_{i=1}^{n} k_i m_i e_{i,material} + \sum_{i=1}^{q} k_i E_i e_{i,energy} \tag{4}$$

where

- n represents the number of types of materials.

- q represents the number of types of energies.
- m_i is i th material consumption in one specific certain period (kg).
- E_i is i th energy consumption in one specific certain period (kWh).
- C_i is the cost of i th materials or energies (\$/kg or \$/kWh).
- e_i is the environmental impacts of i th materials or energies (kg/kg or kg/kWh).
- k_i is aggregation of relevant parameters during calculation.

2.1 Indirect contribution

Constituting a substantial facet of indirect contribution, equipment emerges as an indispensable factor warranting unwavering consideration both in the realm of cost estimation and the evaluation of environmental impacts. Moreover, the spatial dimensions of the edifices are contingent upon the cumulative footprint of the equipment ensemble. Regrettably, there is a dearth of available literature within the domain of Life Cycle Assessment (LCA) that encompasses comprehensive evaluations. That is to say, most researchers often tend to focus primarily on the isolated input-output evaluation of specific industrial processes. In this context, the broader consideration of encompassing both the intricate equipment and the enduring architectural elements tends to be underrepresented or overlooked.

Henceforth, the pivotal focal point in the estimation of costs and the conduct of Life Cycle Assessment (LCA) pertaining to indirect contributions revolve around the strategic handling of equipment considerations.

2.1.1 equipment

Based on established industrial production lines, it becomes feasible to ascertain the equipment composition of the production lines, along with the pertinent parameters with these apparatuses. A comprehensive repository of specifications can be procured through methods including the perusal of official digital platforms, direct engagement with manufacturers to solicit technical manuals, and cultivation of networks within the industry, among other avenues.

Consequently, this concerted effort culminates in the acquisition of detailed and essential particulars, spanning dimensions such as prevailing market valuations, maximum operational capacity, spatial footprint, and lifetime. Furthermore, in instances where certain particulars are not readily accessible—such as specific material compositions, performance attributes, availability, and yield rates—these gaps are bridged through empirically-informed suppositions, often based on the perusal of industrial drawings or dialogues with technical experts.

Within this paradigm, each discrete facet of the production line can be distinctly correlated to a specific equipment entity within the contemporary market landscape, fortified by a wealth of aptly collated information. This systematic approach invariably underpins the realization of exhaustive cost estimation and life cycle assessment, thereby enabling a comprehensive appraisal of indirect contributions.

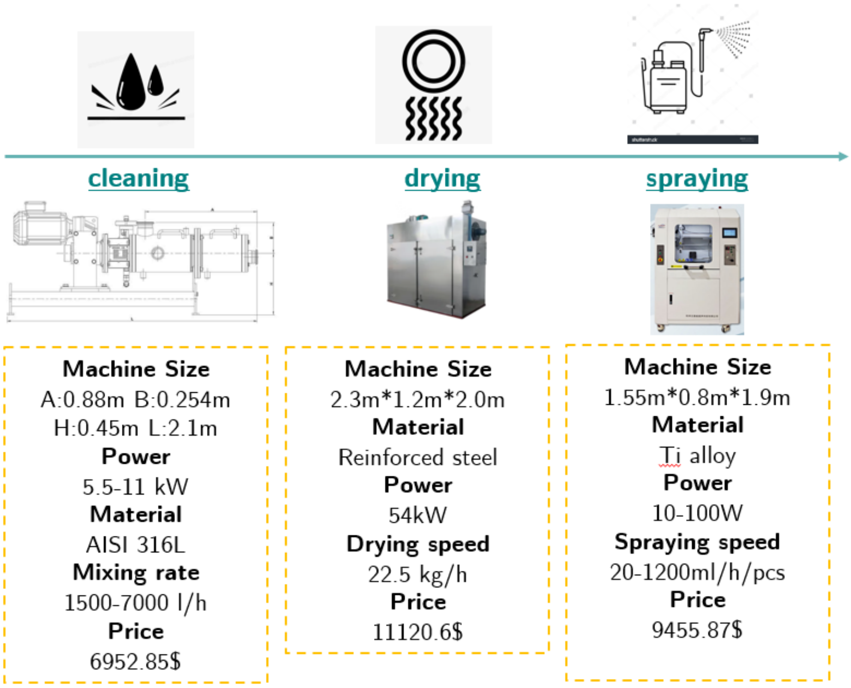

Figure 3: equipment example

Initiating the process of cost estimation and Life Cycle Assessment (LCA) for equipment involves a preliminary stride: the computation of the equipment count. This practice is underpinned by two primary considerations. Firstly, it serves as a foundational step in quantifying the aggregate material input, given that parameters are accessible for individual equipment units. Secondly, the determination of the total equipment count is instrumental in assessing the collective equipment footprint, thereby lending itself to energy appraisal and building areas evaluation.

With the maximum operational capacity already established, the derivation of equipment count is facilitated through a comparative analysis. Specifically, when the annual production attains a quantum denoted as "n_u cells", the quantification of equipment count ensues by juxtaposing the annual production rate vis-à-vis the real throughputs.

$$a_i = \lceil \frac{n_u}{60 v_i T} \rceil \tag{5}$$

where

- a_i is the number of equipment i (1).
- v_i is the throughput of equipment i (unit/min).
- T is the maximum annual operation time (hr/y).

Once the number of equipment units has been determined, it paves the way for subsequent endeavors in cost analysis and life cycle assessment (LCA). Diverse methodologies are employed in these analyses.

Regarding cost considerations, an initial approximation of equipment cost often involves a rudimentary summation of the equipment's purchase price, typically disregarding ancillary expenses such as delivery and installation costs. A more comprehensive formula for calculating equipment cost is represented as follows:

$$C_{equip} = C_{pur,equip} + C_{deli} + C_{install} + C_{instru} + C_{pip} + C_{eng} + C_{constru} + C_{contractor} + C_{contingency} \quad (6)$$

where

- C_{equip} is the total equipment costs ($).
- $C_{building}$ is the total building costs ($).
- $C_{pur,equip}$ is the costs to purchase equipment ($).
- C_{deli} is the freight to deliver equipment ($).
- $C_{install}$ is the costs related to the erection of equipment ($).
- C_{instru} is costs of instrument costs for auxiliary equipment ($).
- C_{pip} is the piping costs ($).
- C_{eng} is the engineer costs of designing the factory ($).
- $C_{constru}$ is the costs of temporary construction and operation and other construction overhead ($).
- $C_{contractor}$ is the costs contractor fee ($).
- $C_{contingency}$ is the contingency costs covers unforeseen events ($).

Nonetheless, a significant challenge lies in the unavailability of precise figures for these ancillary costs. Therefore, a set of factors is employed to estimate these expenditures. Amsterdam conducted a comprehensive literature review on capital cost estimation, employing factorial techniques in his master's thesis[8]. According to his research, the Lang-type factors are recommended as key parameters in our model. Ultimately, we opted to utilize the Lang-type parameters sourced from the work of Peter and Timmerhaus[9]. Notably, this methodology was also employed by the US Department of Energy in a 2015 report focusing on liquid fuel technologies[10].

Table 1: Estimation of capital investment based on purchasing costs of equipment [9]

Costs	Type of equipment		
	Solid-processing	Solid-fluid processing	Fluid-processing
$C_{pur,equip}$	1.00	1.00	1.00
C_{deli}	0.10	0.10	0.10
$C_{install}$	0.45	0.39	0.47
C_{instru}	0.09	0.13	0.18
C_{pip}	0.16	0.31	0.66
C_{eng}	0.33	0.32	0.33
$C_{constru}$	0.39	0.34	0.41
$C_{contractor}$	0.17	0.18	0.21
$C_{contingency}$	0.34	0.36	0.42
C_{equip} **(total)**	3.03	3.13	3.78

In summary, the total cost of equipment is eventually written as below.

$$C_{equip} = \sum_{i=1}^{m} \varepsilon_i P_{eqp,i} \lceil \frac{n_u}{60 v_i T} \rceil \tag{7}$$

where

- ε is the ratio of C_{equip} and $C_{pur,equip}$, which can be obtain in the Table 1. It changes with the type of equipment i.

Additionally, in alignment with insights gleaned from Life Cycle Assessment (LCA) literature pertaining to construction, our model incorporates Building Information Modeling (BIM) due to the analogous roles played by buildings and equipment within our overarching methodological framework[11]. To elucidate further, the comprehensive environmental impacts are categorized into five distinct domains: production, transportation, construction, demolition, and waste treatment, a classification scheme that harmoniously aligns with our overarching methodological schema[12].

$$E_p = \sum_{i=1}^{n} (1 + b_i) * Q_{pi} * e_{pi} \tag{8}$$

$$E_t = \sum_{i=1}^{n} (1 + \gamma) * Q_{ti} * L_{ti} * e_t \tag{9}$$

$$E_c = A_c * P_c * e_{ele} \tag{10}$$

$$E_d = A_d * P_d * e_{ele} \tag{11}$$

$$E_w = \sum_{i=1}^{n} (1 + \gamma) * Q_{wi} * L_w * e_t \tag{12}$$

where

- n represents the number of used equipment materials (1).
- b_i is the waste factor of the i th material (1).
- Q_{pi} represents the used material quantity of ith material (kg).
- e_{pi} is the environmental impact factors of ith materials production, which can be obtained from LCA databases such as ecoinvent (kg Equivalent Gas Emissions/kg).
- γ is the empty return coefficient (1).
- Q_{ti} represents the quantity of ith transported equipment materials (kg).
- L_t is the transportation distance from the factory to the construction site (km).
- A_c is the area of construction site (m^2).
- P_c is the electricity power consumed during construction (kWh/m^2).
- e_{ele} is the environmental impact factors of local electricity supply, which can be obtained from LCA databases such as ecoinvent (kg Equivalent Gas Emissions/kWh).
- A_d is the area of demolition site (m^2).
- P_d is the electricity power consumed during demolition (kWh/m^2).

- Q_{wi} represents the jth wasted material quantity of equipment (kg).
- L_w is the transportation distance from the construction site to the landfill site (km).
- e_t is the environmental impact factors of transportation, which can be obtained from LCA databases such as ecoinvent (kg Equivalent Gas Emissions/kWh).

Another challenge involves the determination of various parameters for these formulas. **daoud_quantifying_20** conducted a study in 2014, quantifying material waste within the Egyptian construction industry and providing a comprehensive analysis of rates and factors. Additionally, **zhang_surface_2014** undertook an analysis of existing buildings. Notably, their findings revealed that energy consumption during the demolition stage represents only 15% of the energy consumed during construction, as per their results.

In this study, waste factors have been set at 0.05 for steel and PVC materials, and 0.025 for all other materials, based on the research outcomes of the aforementioned studies. Furthermore, an empty return coefficient (denoted as γ) of 0.67 has been adopted, in accordance with the LCA research conducted by **hao_carbon_2020**. in 2020. Simultaneously, electricity consumption during on-site construction has been established at 50 kWh per square meter, as per the BIM-based study conducted by **gervasio_macro-component_2014**. for an office building in Western Europe.

Ultimately, the final environmental impacts can be given:

$$e_{total} = \sum_{i=1}^{n} \lceil \frac{n_u}{60 v_i T} \rceil \lceil (1 + b(i)) * Q_{pi} * e_{pi} + 83.5 Q_{ti} * e_t + 57.5 A_c * e_{ele} + 83.5 Q_w * e_t \rceil \tag{13}$$

To provide further clarity, it's evident that variables such as b_i, Q_{pi}, e_{pi}, Q_{ti}, and v_i are inherently determined by the characteristics of the equipment itself. Conversely, variables like e_{ele} are contingent upon the methods of local power generation and supply. Similarly, e_t is contingent on the transportation methods employed.

Regarding Q_w, its value varies depending on the specific material and is calculated using the following formula.

$$Q_w = Q_p * w * L_w * e_t \tag{14}$$

where

- w represents the waste rate of materials (1).

Table 2: some parameters within the environmental impacts calculation

parameters	unit	quantity
γ	/	0.67
waste factor for PVC and steel	/	0.05
waste factor for other material	/	0.025
waste rate of steel	/	10%
waste rate of timber and concrete	/	80%
transportation distance	km	50
electricity consumption	kWh/m^2	50

2.1.2 building

To commence, given that this is a methodological introduction grounded in general conditions, we can assume that the building takes the form of a square structure with a height of 5 meters, wall thickness of 25 centimeters, and two intersecting walls within. Under these assumptions, we can calculate the volume of the walls. Furthermore, our considerations encompass only concrete and steel materials. The reinforcement ratio is established at 1%.

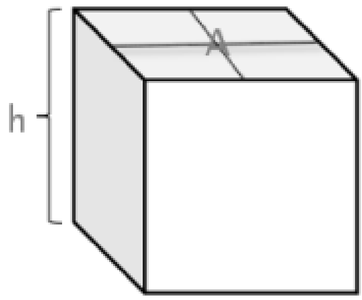

Figure 4: architectural diagram

Similar to equipment, buildings also serve as tubular conduits within our overarching descriptive framework. Consequently, when it comes to Life Cycle Assessment (LCA) results, the methodology employed for computation aligns with that utilized for equipment. However, owing to their distinct functional properties, it is postulated that a manufacturing facility comprises four types of constructions, each tailored to specific functions: manufacturing buildings, storage facilities, open yards, and ancillary buildings. These constructions are unrelated to production lines and encompass facilities such as dormitories and cafeterias for workers. To commence, it may be prudent to initiate the cost calculation first.

$$C_{building} = C_{building}^{man} + C_{building}^{stor} + C_{building}^{anc} + C_{building}^{yard} \tag{15}$$

where

- $C_{building}^{man}$ is the cost of manufacturing buildings ($).
- $C_{building}^{stor}$ is the cost of storage buildings ($).
- $C_{building}^{aux}$ is the cost of ancillary buildings ($).
- $C_{building}^{aux}$ is the cost of yards ($).

Fractional techniques, as employed in the preceding section, are also utilized here to estimate various costs that are otherwise unavailable. It's worth mentioning that land costs and envelope costs are computed as reference points in this context.

$$C_{building}^{type} = C_{land}^{type} + C_{env}^{type} + C_{elec}^{type} + C_{yard}^{type} + C_{serve}^{type} \tag{16}$$

where

- C_{land}^{type} is the land costs of buildings ($).
- C_{env}^{type} is the costs of envelopes ($).

- C_{elec}^{type} is the costs of electrical systems in the buildings (\$).
- C_{yard}^{type} is the cost of yards, consisting of fencing, sidewalks, etc. (\$).
- C_{serve}^{type} is the costs of service facilities such as the cafeteria or dressing room (\$).

Table 3: Estimation of capital investment based on land costs of constructions [9]

Costs	Type of constructions			
	Manufacturing building	Storage building	Ancillary building	Yard
C_{land}^{type}	1.00	1.00	1.00	1.00
C_{elec}^{type}	1.67	1.67	1.67	0.00
C_{yard}^{type}	0.00	0.00	0.00	2.17
C_{serv}^{type}	0.00	0.00	6.67	0.00
$C_{building}^{type} - C_{env}^{type}$	2.67	2.67	9.34	3.17

As indicated in Table 3, the estimation process is predicated on the land cost, which is contingent upon the building area. Citing findings from the US Department of Energy[13], it is noted that the operational area is 3.5 times larger than the equipment's footprint, while the total floor area is 2.5 times larger than the operational area. Consequently, it becomes imperative to conduct a survey of each equipment's footprint and derive the quantities of each equipment based on the equilibrium equation 5 to ascertain the total equipment footprint. Through this methodology, a correlation between volume and building cost is established.

Furthermore, by scrutinizing environmental impact reports from several electrolyzer manufacturing facilities [14][15], we have acquired area ratios for various types of buildings. These parameters, as delineated in Table 4, are instrumental in the computation of building areas and associated costs.

Table 4: Area ratio of four types of constructions

	Manufacturing building	Storage building	Ancillary building	Yard
Ratio	54.6%	22.9%	14.0%	8.50%

The calculation of envelope costs is approached individually, given its non-linear relationship with area. Envelopes encompass not only walls but also ceilings, and their costs escalate with volume. Both the shape and height of the buildings exert an influence on the rate of cost escalation. In a generalized context, we posit that all structures are cuboids with two intersecting walls. The hypothetical building's height is set at 5 meters, and its base is considered as a square. Equation 17 delineates the envelope costs, and Figure 6 provides a clear visual representation, illustrating that the cost of the envelope increases at a slower pace as the building area expands.

$$C_{env}^{type} = P_{env}(A + 4h\sqrt{A}) \tag{17}$$

where

- A is the floor area (m^2).
- h is the height of buildings (m).
- P_{env} is the costs of per unit volume of envelope (\$/m^2).

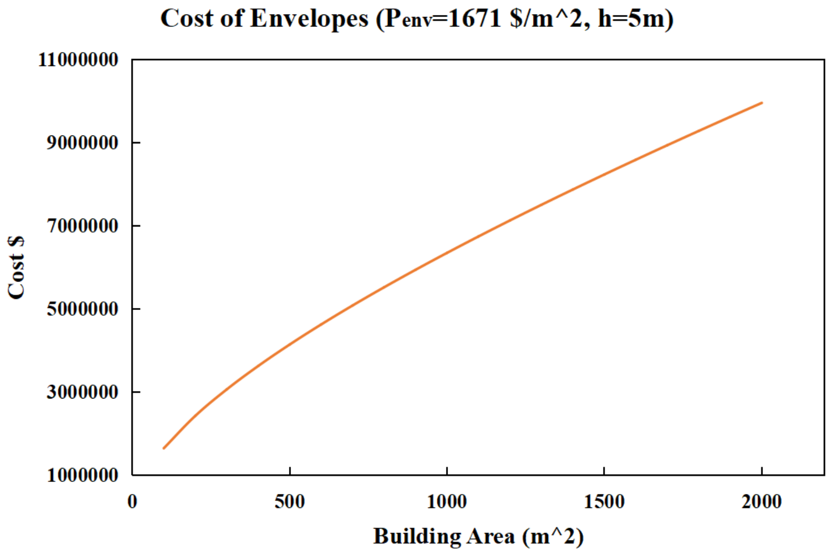

Figure 5: Envelope costs of buildings of different building areas

The Equations 20 is the mathematical form of the overall building cost.

$$C_{building} = P_{env}(14.7A_{equip} + 13.6h\sqrt{A_{equip}}) + 58.4P_{land}A_{equip} \tag{18}$$

$$A_{equip} = \sum_{i=1}^{k} a_i A_i \tag{19}$$

- A_{equip} is the sum of machine's footprint (m^2).
- P_{land} is the price of land ($\$/m^2$).
- k is the number of machine types (1).
- A_i is the footprint of machine i (m^2).

In the context of performing Life Cycle Assessment (LCA) for buildings, as previously elucidated, we shall persist in the utilization of the Building Information Modeling (BIM) approach. Concurrently, when coupled with the classification schema for various building types, the derivation of environmental impact assessments unfolds through the following delineated calculation, as exemplified by the computation of carbon footprints:

$$e_{building} = 4125\sqrt{A} + 9.77A \tag{20}$$

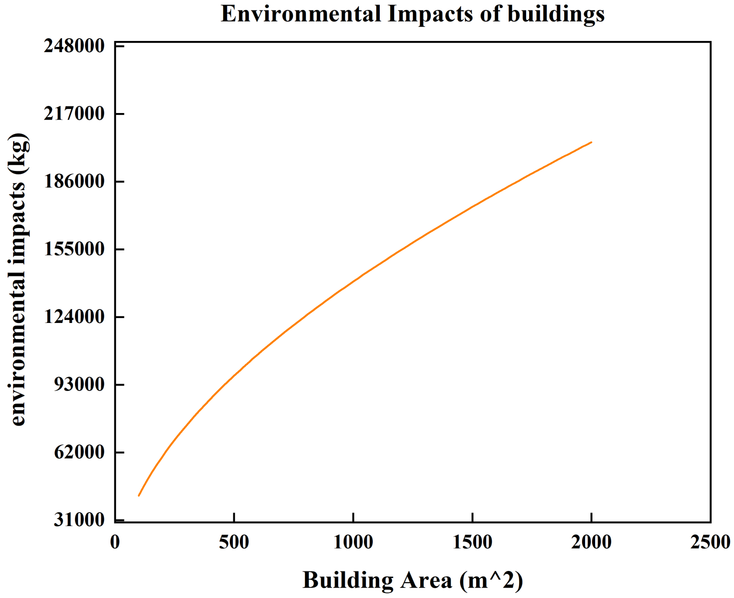

Figure 6: Environmental impacts of buildings of different building areas

2.2 direct contribution

Direct contribution, as the term implies, denotes the immediate allocation of energy and materials to the production process. Whether in the realm of life cycle assessment or cost estimation, these two variables have consistently remained the focal point and foremost concern of most research endeavors. Drawing upon an extensive body of related literature, it becomes evident that the crux of conducting a successful Life Cycle Assessment (LCA) or cost estimation boils down to two fundamental steps: the determination of material and energy consumption, and the acquisition of material prices and environmental impact factors.

Diverging from conventional research paradigms, our comprehensive model, inspired by economic principles, places a particular emphasis on the concept of scale effects. In essence, rather than examining an industrial process with a static lens or utilizing constants to represent variables like material prices, this model centers on establishing the intricate relationship between product pricing and production scale. In a broader context, since price can be regarded as an inherent dimension within life cycle assessment, the inference of scale effects is also expansively applicable to LCA.

2.2.1 material

Raw materials constitute the foundational cornerstone of every production process, serving as the pivotal starting point. Drawing upon insights gleaned from scientific papers and industrial reports, material consumption per unit of product can be rigorously evaluated. Moreover, the model accommodates for material losses during production and quantifies material consumption while factoring in material efficiency. This efficiency is explicitly defined as the ratio between the minimum material required and the actual material consumption. It's noteworthy that as plant size progresses, material efficiency may exhibit a gradual increase but eventually reaches an asymptotic limit. Nevertheless, this model does not account for the growth trend in material efficiency due to limitations in available data. Consequently, the total material costs are presented in three distinct components:

$$\eta_{m,i} = \frac{M_{i,min}}{M_{i,actual}} \tag{21}$$

$$C_{material} = C_{raw} + C_{waste} + C_{supp} = \sum_{i=1}^{k} \frac{M_{i,min}}{\eta_{m,i}} P_{m,i} + C_{supp} \tag{22}$$

where

- $\eta_{m,i}$ is the material efficiency of i.
- $M_{i,min}$ is the minimum amount of material i required for producing one unit of product (kg).
- $M_{i,actual}$ is the actual amount of material i required for producing one unit of product (kg).
- C_{raw} is the raw material cost ($/unit).
- C_{waste} is the cost of material wasted or scraped ($/unit).
- C_{supp} is the cost of materials that are not considered raw but necessary in production such as protective clothing for operators ($/unit).
- $P_{m,i}$ is the unit price of material i ($/kg)

The annual cost associated with material procurement is presumed to be 0.9% of the total investment denoted as C_{IC}[16], as outlined in reference. This assumption is predicated on the close correlation between this cost and the scale of the plant. In addition to this, the determination of raw material costs necessitates information regarding both the consumption rates and prices of the raw materials in question.

This table provides a comprehensive overview of the prices, along with the corresponding order quantities, for three raw materials. This data has been compiled from vendors by Scataglini[17]. Notably, the table illustrates a marked downward trajectory in prices over time.

Table 5: Anode-supported cell material prices [18]

Material	Order quantity (kg)	Price ($/kg)
NiO powder	1	68.5
	5	42.5
	10	37
	20	34
8YSZ powder	1	139.2
	5	115.8
	10	94.5
	50	71.6
	100	49.7
	1000	35.2
	10000	29.8
LSM powder	100	170
	1000	95
	10000	70

Evidently, it is apparent from this table that a relationship exists between materials and order quantity. In simpler terms, as the purchasing volume increases, the unit price of the material tends to decrease. This observed trend allows for the derivation of an explanatory formula through the introduction of a "learning rate."[19]

$$Y = AX^{\beta} \tag{23}$$

$$\beta = log(m)/log(2) \tag{24}$$

where

- Y is the cost per unit (\$/unit).
- A is the cost for the first unit (\$/unit).
- X is the number of units (1).
- β is the exponential or the slope of the learning curve.
- m is the learning rate.

The learning rate, in this context, serves as an indicator of the rate at which the price diminishes. Specifically, when the order volume doubles, the price experiences a reduction by a factor of m. Nevertheless, it's important to acknowledge that in many instances, the price quotations for materials are treated as confidential, making it impossible to compute the precise value of m. Consequently, default values for m must be established. Subsequently, raw materials are categorized into four distinct subgroups denoted as R_1, R_2, R_3, and R_4.

- Materials categorized within R_1 pertain to custom-built materials that are exclusively employed in factory f_j, such as specific component solvents. For these materials, the annual production volumes align with their purchasing volumes, consequently leading to a sensitive decrease in price quotations as purchasing volumes increase. In this context, the default value for m has been established at 0.8.

$$P_{m,i} = p(S_{i,f_j}), \forall r \in R_1 \tag{25}$$

- Materials categorized within R_2 encompass those that are commonly employed within specific industries, adhering to standardized type numbering rules. A classic example includes Nafion membranes used in the production of PEM (Proton Exchange Membrane) electrolyzers. In the case of these materials, price quotations likewise fluctuate in response to order volumes, although at a more gradual rate. This is because the influence of a single factory typically exerts a minimal impact when compared to the broader industry. Consequently, the default value for m within this category is defined as 0.9.

$$P_{m,i} = p(S_{i,F}) = p(\sum_{j=1}^{l} S_{i,f_j}), \forall r \in R_2 \tag{26}$$

- Materials classified within R_3 are universally utilized across diverse industries, including metals, and are therefore not significantly influenced by the operations of a single factory. In the majority of instances, the price dynamics of these materials are publicly available and easily accessible online.

$$P_{m,i} \not\propto S_{i,f_j}, \forall r \in R_3 \tag{27}$$

- Materials categorized within R_4 are characterized as rare materials with limited and fixed reserves. In some instances, the prices of these materials may even experience an increase in response to higher order quantities, a phenomenon attributed to their scarcity and limited availability.

where

- p is the correlation between the material price and the order volume.
- F is the set of factories. $F = \{f_1, f_2, f_3, ..., f_l\}$
- S_{i,f_j} is the order volume of material i from f_j (kg).

Furthermore, it's crucial to acknowledge that prices cannot infinitely decline. For instance, consider the price of Nafion membrane, which stands at $700\$/m^2$ for a purchase volume of 38,250 m^2. When the purchase volume doubles, the unit price decreases to $525\$/m^2$, as illustrated in graph 7. However, it has been observed that when the purchase volume reaches six times the initial volume, the unit price drops to less than half of the original price, a scenario that is both illogical and unrealistic. Therefore, it is imperative to introduce a minimum price threshold into this model. As a result, Equation 23 has been refined to Equation 28.

$$Y = Max(AX^{\beta}, \epsilon A) \tag{28}$$

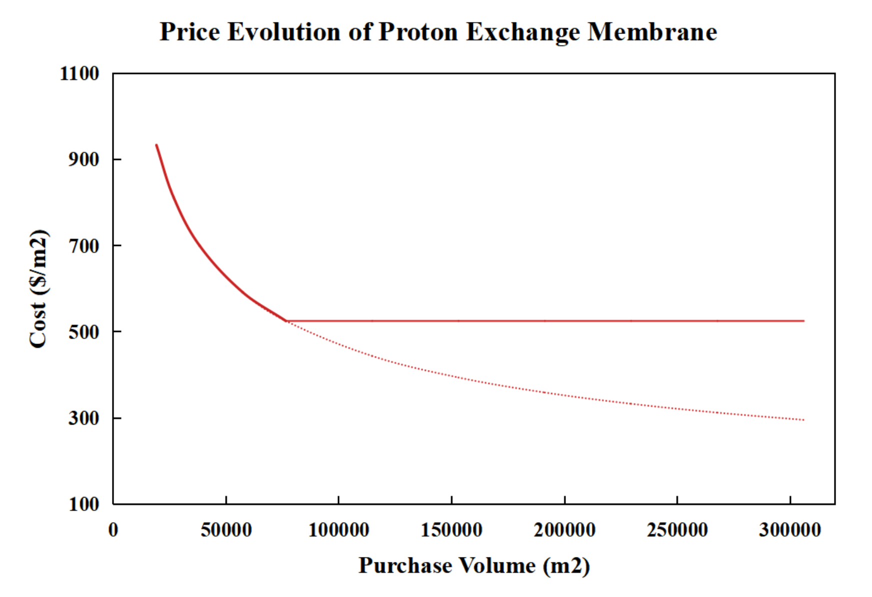

Figure 7: Price evolution of proton exchange membrane with different purchase volumes

where

- ϵ is the factor of minimum price (1). It can be set to be equal to m, or set to a value such as 50%.

Total material costs can ultimately be written as the following equation.

$$C_{material} = \sum_{i=1}^{k} \frac{M_{i,min}}{\eta_{m,i}} P_{m,i}^{i} Max((\frac{n_u}{n_{u,i}})^{\beta}, \epsilon A) + 0.009 \frac{C_{IC}}{n_u} \tag{29}$$

where

- $P_{m,i}^{i}$ is the initial price of material i at production rate of $n_{u,i}$ ($/kg).

Regarding environmental impacts, rather than incorporating a learning rate, an alternative approach involves conducting comprehensive upstream lifecycle assessments to acquire the environmental impact factors. In alignment with the classification provided earlier, the environmental impact factors for most materials can be directly sourced from the existing Life Cycle Assessment (LCA) database. However, for materials like Nafion, a distinct methodology is adopted. In such cases, Nafion is treated as a product in itself, undergoing a comprehensive life cycle assessment "from cradle to gate" to derive its specific environmental impact factor.

2.2.2 energy

In this context, the concept of "energy" extends beyond traditional forms like electricity to encompass labor as well. Labor, in a broader sense, is considered a form of energy input. This encompasses not only direct operational labor but also encompasses the entire workforce, including administrative, engineering, and other support personnel within the company.

$$C_{labor} = C_{directMP} + C_{R\&D} + C_{eng} + C_{overhead} + C_{admin} \tag{30}$$

- $C_{directMP}$ is the costs of direct manufacturing labor ($\$/unit$).
- $C_{R\&D}$ is the costs of R&D personnel ($\$/unit$).
- C_{eng} is the costs of engineers ($\$/unit$).
- $C_{overhead}$ is the overhead cost that takes to run ancillary services such as cafeteria and safety ($\$/unit$).
- $C_{directMP}$ is the costs of administrative personnel ($\$/unit$).

When calculating the costs associated with direct manufacturing labor, several key factors come into play. These include the number of workers, the annual working hours, and the labor cost per hour. It is assumed that workers are continuously employed while the machines are in operation. The maximum annual working time is set at 6,000 hours, but in practice, machines may stop once the annual production target is achieved. Additional workers are hired when the annual production rate increases. However, it's important to note that the number of workers does not necessarily grow linearly with production volume, as one employee can oversee one or multiple machines, especially on automated production lines.

Reference [19] provides a function to express the relationship between operating labor and plant capacity. The exponent of 0.226 in Equation 31 has been derived from Figure 8.

$$N_{auto} = N_{i,auto}(\frac{a_i}{a_i^i})^{0.226} \tag{31}$$

where

- N is the present number of workers (1).
- $N_{i,auto}$ is the initial number of workers (1).
- a_i^i is the initial number if equipment i (1).

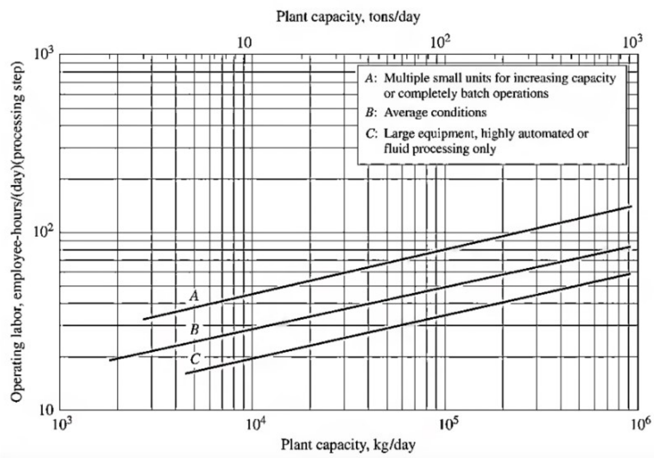

Figure 8: Operating labor requirements in the chemical process industry[2]

In Figure 9, both lines depict the relationship between labor and production volume. The dashed line represents the labor pattern for traditional manual processes, indicating linear growth in labor demand as production increases. Conversely, the solid line represents labor demand in automated processes and shows an exponential correlation. Notably, this solid line is significantly lower than the dashed line, indicating a substantially reduced need for labor in automated factories. Furthermore, labor demand in automated plants exhibits a slower rate of growth, particularly at higher annual production rates.

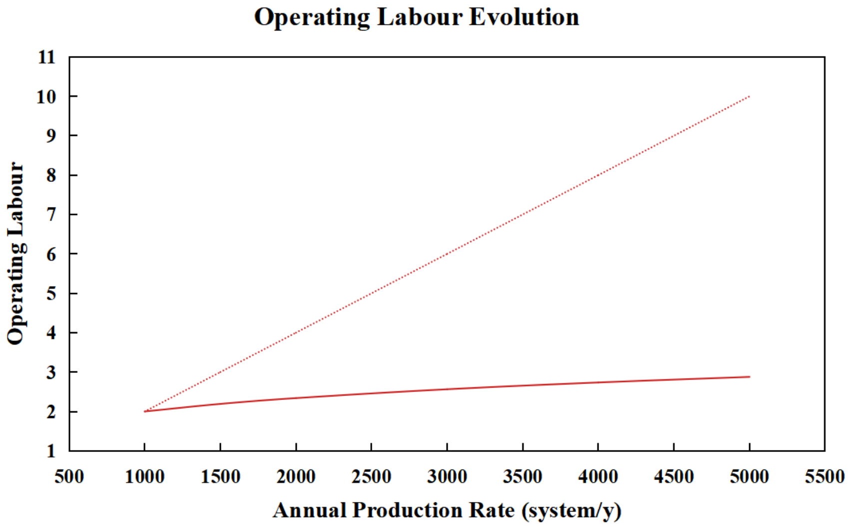

Figure 9: Operating labor requirements evolution with annual production rate

Following the identical method for capital costs, the labor costs are finally expressed in Equation 32, where the price of labor is extracted from online databases.

$$C_{labor} = 2.17 C_{directMP} + 0.047 \frac{C_{IC}}{n_u} \tag{32}$$

$$C_{directMP} = P_{labor} \sum_{i=1}^{k} \frac{n_u}{60 v_i} (N_{i,auto} (\frac{a_i}{a_i^i})^{0.226} + N_{i,man} \frac{a_i}{a_i^i}) \tag{33}$$

where

- P_{labor} is the price of labor (\$/person·h).
- $N_{i,man}$ is the initial number of workers for manual equipment (1).

In the context of conventional energy consumption, electricity is categorized into two distinct types: operational electricity and maintenance electricity. Given that the unit price of electric energy and its associated environmental impact factors tend to remain relatively constant, the primary focus lies in determining the consumption of electricity.

In the case of operational electricity, its calculation is carried out using the following formula:

$$E_{ele} = \sum_{i=1}^{n} \lceil \frac{n_u}{60 v_i T} \rceil * t_i * P_i \tag{34}$$

where

- P_i is the power rate of equipment i (kW).
- t_i is the operation duration within one year of the machine (h).

Assuming an average building maintenance electricity consumption of 34.4 kWh per square meter, the calculation for maintenance electricity can be expressed as follows:

$$E_{ele} = \sum_{i=1}^{n} \lceil \frac{n_u}{60 v_i T} \rceil * A_i * 34.4 \quad (35)$$

Hence, the overarching formula for cost estimation and environmental impact assessment can be expressed as follows:

$$e_{elec,total} = \frac{e_{elec}}{n_u} (\sum_{i=1}^{n} \lceil \frac{n_u}{60 v_i T} \rceil * t_i * P_i + \lceil \frac{n_u}{60 v_i T} \rceil * A * 34.4) \quad (36)$$

3 Case Study

3.1 PEMEC

The first PEM electrolysis was introduced by Grubb [20] in the early fifties. It employs H^+ as an ionic agent and solid polysulfonated membranes (Nafion®, fumapen®), which have low gas permeability, high proton conductivity, low thickness and high-pressure operations, as electrolyte. Normally PEM electrolysis cells (PEMECs) work at temperatures between 50-95 °C. Recent progress in polymeric membranes with protonic conductivity operative at temperatures up to 200 °C has been carried out in the field of fuel cell technology and extended the temperature for PEM electrolyzers as well [21].

Compact system design is possible for PEMEC and SOEC thanks to their solid electrolyte. A PEM stack consists of repeating cells that are electrically connected in series. The core component of each cell is the catalyst-coated membrane, which is the polymer membrane applied with cathode and anode catalysts on two sides respectively. The porous transfer layers (PTLs) help enhance the transfer of water and gas on the surfaces of the membrane. CCM and PTLs sealed by resin frame represent the membrane electrode assembly (MEA). Thick metal plates, which are also called end plates are added to both ends of the stack to structurally hold the cells. Bipolar plates separate cells in the stack. The channels on them also facilitate the transport and collection of water and gas. Table 6 listed the material chosen for each component of PEMEC. Typically, the cost of balance of plant (BOP) of both PEMEC and SOEC is not included in this study, as they vary with the capacities of the electrolyzers, which are also excluded to normalize the cost to $/kW and to disentangle the EOS.

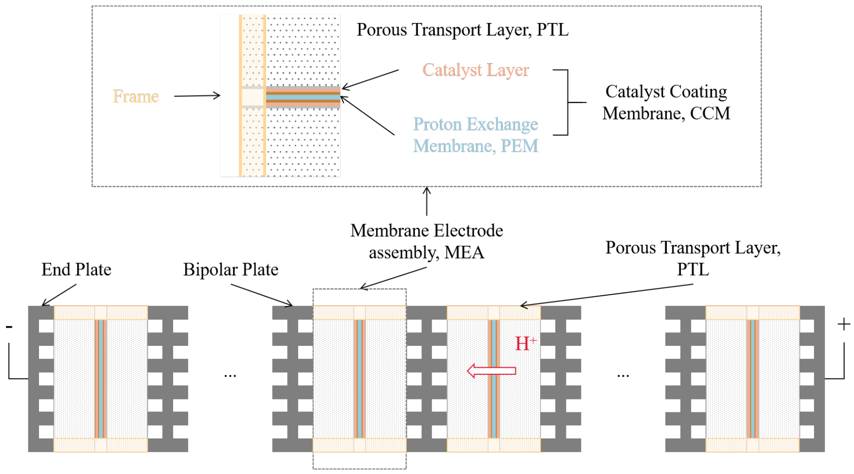

Figure 10: Structure of PEMEC

Table 6: PEMEC components [22]

Components	Material
Membrane	Nafion 117
Catalyst	7 g/m^2 Pt (Anode), 4 g/m^2 Pt-Ir (Cathode)
PTL	Sintered porous titanium (coated with gold) (Anode), Cabon paper (Cathode)
Frame	PPS-40GF
Bipolar Plate	Stainless Steel 316 Sheets (coated with gold)

Table 7: Functional specification of the PEM electrolysis system and SOE system [22][18]

	Value		Unit
	PEMEC	SOEC	
Total plate area	967	329	cm^2
Active Area	680	299	cm^2
Current Density	1.7	0.9	A/cm^2
Reference Voltage	1.7	1.3	V
Power Density	2.89	1.17	W/cm^2
Single Cell Power	1965.2	349.83	W
Cell / Stack	255	130	
Stack power	500	45	kW
Stack / System	2	1	
System Power	1000	45	kW

Therefore, the manufacturing of PEMEC can be divided into five parts. The processing procedure is shown in Figure 11

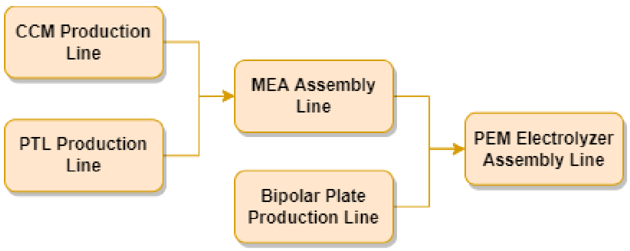

Figure 11: Structure of PEMEC manufacturing lines

3.1.1 CCM Production Line

Figure 12 portrays a schematic representation of the Critical Component Manufacturing (CCM) process. Initially, the Nafion membrane undergoes an unrolling procedure, followed by the application of catalyst material via spray nozzles, a method chosen for this particular case study. It is noteworthy that catalyst deposition techniques encompass spray coating, screen coating, slot-die coating, and doctor blade coating. In the context of this study, spray coating is the selected approach.

The necessity for Platinum-group metals (PGMs) as catalysts arises due to their suitability for handling the demanding operational conditions within Proton Exchange Membrane Electrolyzer Cells (PEMECs). Notably, these conditions encompass high current densities and a highly acidic environment with a pH of approximately 2. This unique operational environment contributes significantly to the elevated cost of PEMECs.

Following the catalyst deposition, the membrane undergoes a drying and cooling process. To maintain the quality of the catalyst coatings, an optical monitoring system is employed throughout the production process. Subsequently, the coating procedure is replicated on the opposite side of the membrane. Lastly, the CCM is sectioned into discrete components and routed to the Manufacturing of Electrode Assemblies (MEA) production line.

This delineation encapsulates the key operational steps within the CCM production process, marked by a focus on catalyst deposition and quality control measures in the fabrication of critical components for PEMECs.

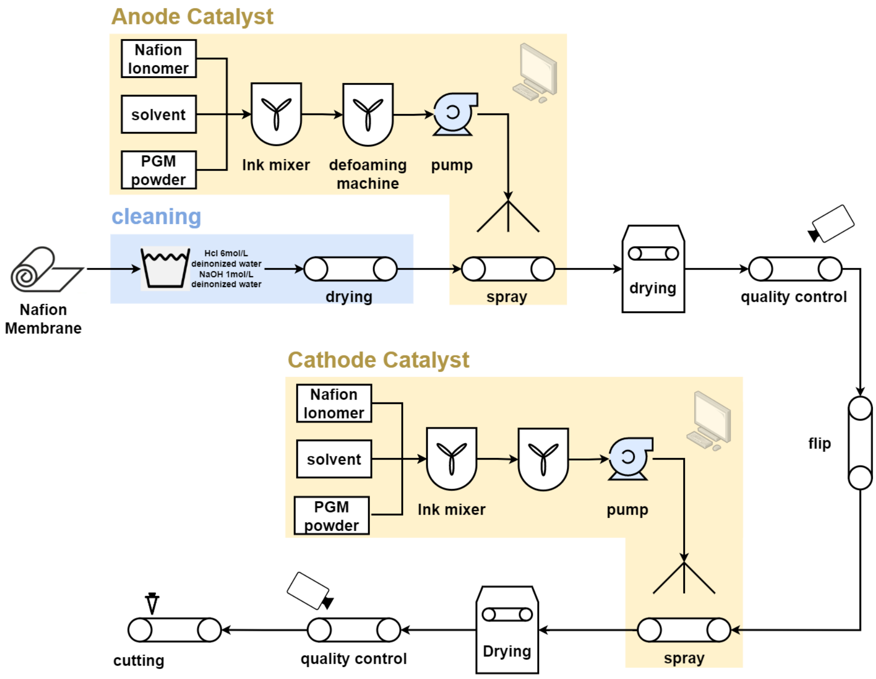

Figure 12: Process flow for CCM manufacturing

3.1.2 PTL Production Line

In a similar vein, Proton Transport Layers (PTLs) employed in Proton Exchange Membrane Electrolyzer Cells (PEMECs) necessitate exceptional corrosion resistance. These layers can be fabricated using either sintered titanium through powder metallurgy or carbon paper. Figure 13 illustrates the procedural workflow for manufacturing cathode and anode PTLs. In our specific scenario, the anode PTL is constructed from sintered titanium, while the cathode PTL is fashioned from carbon cloth.

The manufacturing process commences with the amalgamation of titanium powder with adhesive powder and lubricants, which serve to facilitate the compaction of these inherently brittle particles. These compacts subsequently undergo sintering within a furnace. During this sintering phase, the particles experience a melting process, leading to the creation of porous structures within the material. Ultimately, to curtail contact resistance and inhibit oxidation, these components receive a coating of precious metals like gold and platinum through the process of physical vapor deposition (PVD).

On the cathode side, when carbon paper or carbon cloth is procured from vendors, the sole requisite procedure entails the precise cutting of these materials to conform to the specified dimensions.

This elucidation offers insights into the critical steps underpinning the fabrication of both anode and cathode PTLs within the context of PEMECs, where materials and processes are meticulously selected to meet the demanding corrosion resistance criteria.

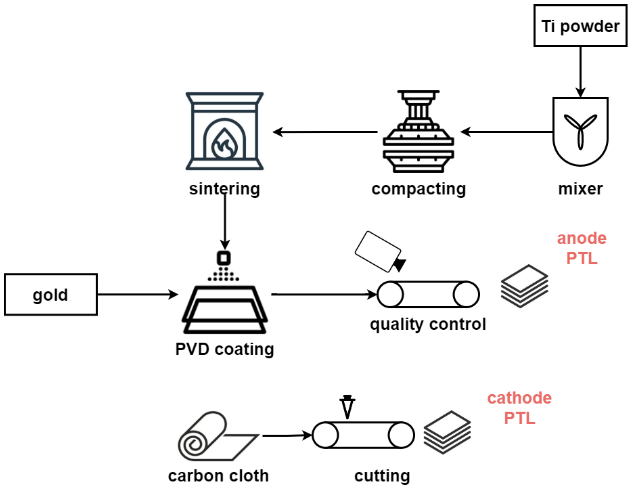

Figure 13: Process flow for PTL manufacturing

3.1.3 MEA Production Line

Within this manufacturing process, the Proton Transport Layers (PTLs) and Critical Component Manufacturing (CCM) components are securely encapsulated using a polyphenylene sulfide (PPS) resin blend infused with 40% glass fiber. This composite frame serves a dual purpose: it acts as a robust enclosure to house the Membrane Electrode Assembly (MEA) while also affording the necessary flexibility to function effectively within the harsh and corrosive operating environment characteristic of Proton Exchange Membrane Electrolyzer Cells (PEMECs). The chosen manufacturing technique for this frame is injection molding.

Injection molding is the method of choice for shaping the PPS resin mixed with glass fiber into the desired frame structure. This approach allows for precision in crafting complex geometries and ensuring a secure and robust seal around the PTLs and CCM components. It is particularly well-suited for creating parts that must endure the demanding conditions and stringent performance requirements encountered in PEMECs.

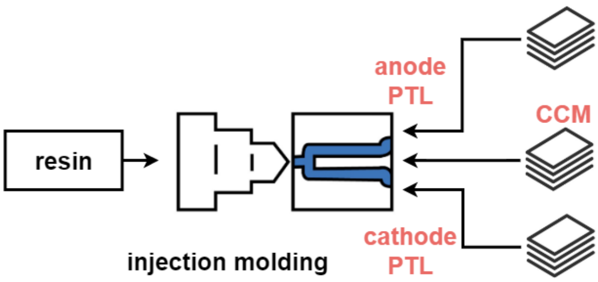

Figure 14: Process flow for MEA manufacturing

3.1.4 Bipolar Production Line

Materials characterized by robust corrosion resistance, such as stainless steel and carbon composites, are the preferred choices for the construction of bipolar plates in Proton Exchange Membrane

Electrolyzer Cells (PEMECs). As elucidated in Figure 15, the manufacturing process unfolds in a subsequent manner:

The initial step entails the transformation of stainless steel coils into blank bipolar plates. Subsequently, intricate channels for the conveyance of gases and water are meticulously stamped onto both sides of these plates. This precise stamping operation serves as a pivotal enabler for the controlled distribution of gases and fluids within the PEMEC system.

To further augment both electrical conductivity and corrosion resistance, an exceedingly thin layer of precious metals, exemplified by gold, is meticulously deposited onto the surfaces of the bipolar plates. This deposition process is achieved through the precise technique of Physical Vapor Deposition (PVD).

In sum, the systematic fabrication of bipolar plates from materials renowned for their corrosion-resistant properties, coupled with the application of a thin and protective precious metal coating via PVD, serves as a fundamental process underpinning the reliability and endurance of these pivotal components within the intricate framework of PEMEC technology.

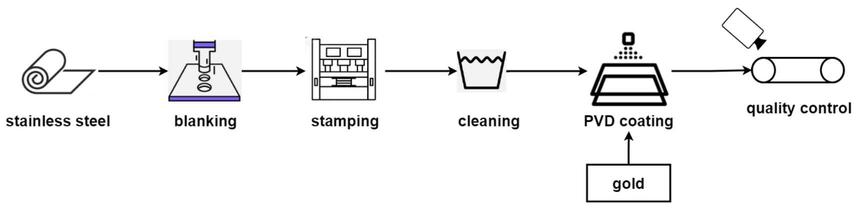

Figure 15: Process flow for bipolar plate manufacturing

3.1.5 PEM Electrolyzer Assembly Line

The assembly process is divided into two distinct segments: the cell assembly line and the stack assembly line. Initially, a single bipolar plate is paired with one Membrane Electrode Assembly (MEA), resulting in the creation of a discrete unit comprising PEM cells. These individual cells are subsequently interconnected in series to assemble a functioning electrolyzer stack.

Presently, the majority of electrolyzer stack assembly lines rely on manual operations, wherein skilled workers undertake tasks that involve stacking, aligning, and connecting various components to produce the electrolyzer stack [22]. However, in light of the escalating demand for green hydrogen and electrolyzers, manufacturers are poised to make substantial investments in augmenting the level of automation within assembly lines and across various facets of production.

This strategic shift towards automation is expected to streamline production processes, enhance efficiency, and ensure consistent quality while accommodating the burgeoning market demand for environmentally sustainable hydrogen and advanced electrolyzer technologies.

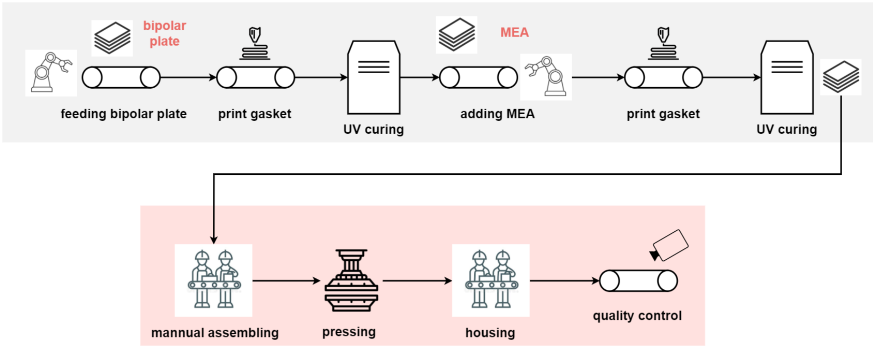

Figure 16: Process flow for PEMEC assembly line

3.2 SOEC

The Solid Oxide Electrolyzer Cell (SOEC) technology traces its origins back to pioneering work conducted in the 1980s by Donitz and Erdle [23]. SOECs are characterized by their operation at elevated temperatures, typically exceeding 500 degrees Celsius, and their capacity to split water in the form of steam. Notably, SOECs are renowned for their potential to efficiently convert electrical power into hydrogen, boasting nearly 100% efficiency. This remarkable efficiency can be attributed to several factors, including lower operating voltage, enhanced kinetics at high temperatures, and the prospect of heat recovery through integration with exothermic processes [24].

Traditionally, SOECs employ O^{2-} ions from yttria-stabilized zirconia (YSZ) as the ionic conductor within the cell. Nevertheless, recent developments have witnessed the emergence and refinement of ceramic proton conductors, owing to their superior ionic conductivity and heightened efficiency, particularly within the intermediate temperature range of 500-700 degrees Celsius [25].

The structural configuration of SOECs bears a resemblance to that of Proton Exchange Membrane Electrolyzer Cells (PEMECs), although the manufacturing processes are notably more straightforward (see Figure 17). Central to the SOEC architecture is the Electrolyte and Electrode Assembly (EEA), which combines the electrolyte and electrodes into a cohesive unit. This EEA represents the core element of SOEC technology.

Given that SOEC technology is still in its nascent stages, its structural designs can vary. In this specific case, we presume the use of anode-supported cells [18]. In such cells, the anode layer possesses greater thickness, approximately 700 micrometers, serving both as an electrode and a structural support for the electrically active components.

The assembly of the EEA is accomplished by sealing it with glass, and the EEA, glass seal, and interconnect collectively constitute the repetitive building blocks within SOEC stacks. This configuration underscores the dynamic and evolving nature of SOEC technology as it advances towards broader commercialization and practical applications.

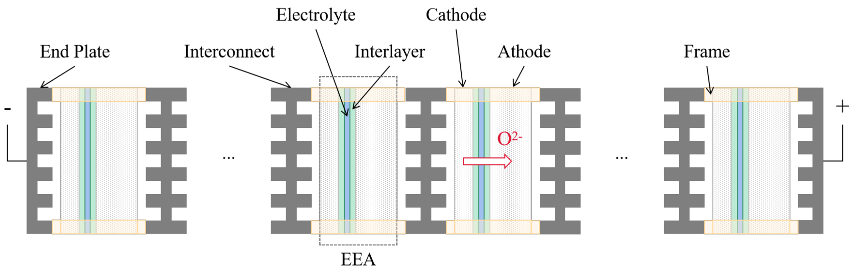

Figure 17: Structure of SOEC

Table 8: SOEC components [18]

Components	Material
Anode	LSM
Anode-electrolyte Interlayer	50% YSZ, 50% LSM
Electrolyte	YSZ
Electrolyte-cathode Interlayer	50% YSZ, 50% NiO
Cathode	Ni/YSZ
Glass Seal	Barium-calcium-aluminosilicate (BCAS)
Interconnect	Stainless Steel 441 or Crofer 22 APU

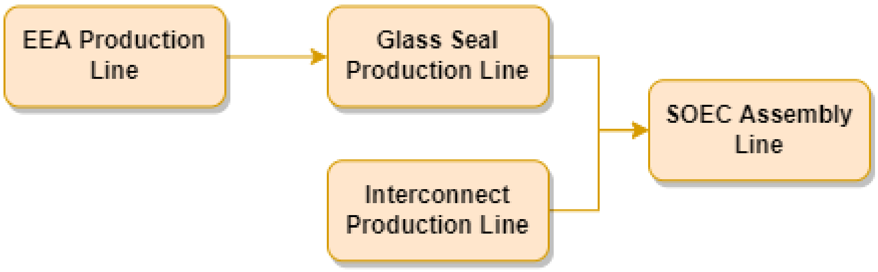

Figure 18: Structure of SOEC manufacturing lines

3.2.1 EEA Production Line

The Electrolyte and Electrode Assembly (EEA) comprises a total of five distinct layers, each serving a specific function within the assembly. These layers are as follows:

1. **Anode Functional Layer:** The Anode Functional Layer is the foundational layer of the EEA, established first to provide structural support for the layers above. It serves as the substrate for the subsequent layers.

2. **Anode-Electrolyte Interlayer:** Positioned above the Anode Functional Layer, the Anode-Electrolyte Interlayer plays a vital role in facilitating communication between the anode and electrolyte layers.

3. **Electrolyte Layer:** Situated atop the Anode-Electrolyte Interlayer, the Electrolyte Layer acts as the ionic conductor within the cell, facilitating ion transport across the electrolyte.

4. **Electrolyte-Cathode Layer:** Above the Electrolyte Layer, the Electrolyte-Cathode Layer interfaces with the cathode layer and plays a pivotal role in enabling the electrochemical processes within the cell.

5. **Cathode Functional Layer:** The topmost layer of the EEA, the Cathode Functional Layer, is essential for efficient oxygen reduction, a crucial process in SOEC operation.

To optimize gas diffusion near the electrolyte, the Anode Functional Layer must exhibit high porosity. Achieving this porosity involves incorporating pore formers, binders, and plasticizers into the anode slurry during the slurry formulation process. Subsequently, the slurry is cast onto a carrier film, and after undergoing infrared drying, the carrier film is removed, leaving behind a green tape that is then trimmed to the requisite dimensions.

The assembly process continues with the application of the remaining four layers onto the substrate. To securely bond these layers together, the mini-stack undergoes a 24-hour furnace treatment at high temperatures ranging between 1300-1400 degrees Celsius. It is crucial to exercise meticulous temperature control during this step to minimize potential chemical interactions between layers and to prevent distortion of the essential porous structure necessary for efficient SOEC operation.

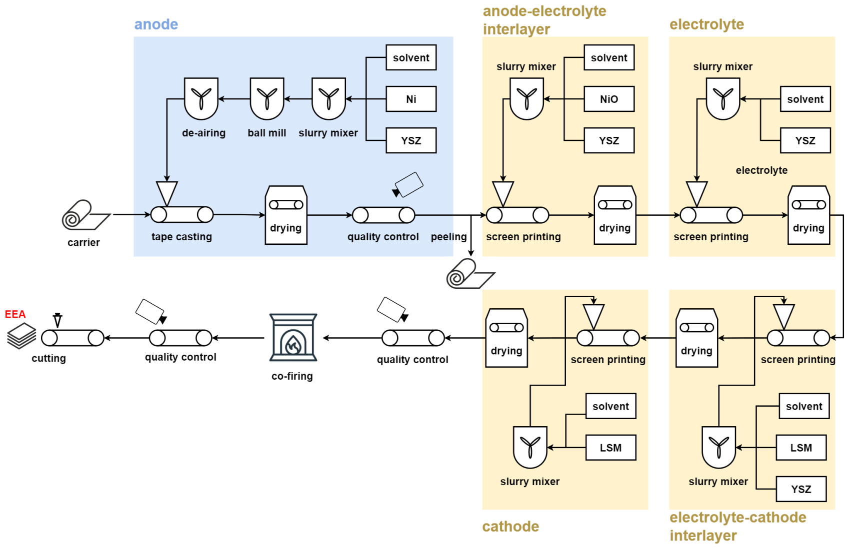

Figure 19: Process flow for EEA manufacturing

3.2.2 Interconnect Production Line

Similar to bipolar plates in Proton Exchange Membrane Electrolyzer Cells (PEMECs), interconnects in Solid Oxide Electrolyzer Cells (SOECs) serve a dual purpose by providing both electrical connections and pathways for gas and water. In this particular investigation, interconnects are meticulously crafted from stainless steel 441. The manufacturing process follows a sequential procedure:

The stainless steel coil is initially subjected to precise stamping using a dual die stamper. This stamping process imparts the desired shape and structure to the plates, forming them into interconnects.

Subsequently, these interconnect plates undergo a crucial enhancement step where they are coated with a layer of manganese cobalt oxide (MCO) spinel. The application of this protective coating is accomplished through cathodic arc plasma vapor deposition (Arc-PVD). It is essential to note that this coating is selectively applied to only one side of the interconnect plates. This strategic application serves several pivotal purposes:

- **Chromium Poisoning Prevention:** The coating on one side serves as a robust barrier, shielding neighboring cells from potential chromium contamination. - **Performance Enhancement:** The incorporation of the MCO spinel coating substantially augments the performance characteristics of the interconnects, contributing to their overall efficacy within the SOEC system. - **Enhanced Durability:** Crucially, the coating bolsters the overall durability of the interconnects, ensuring their sustained functionality over an extended operational lifespan.

This meticulous manufacturing process culminates in the production of interconnects that play a vital role in ensuring efficient electrical connections and facilitating the seamless flow of gases and water within the SOECs. Concurrently, these interconnects act as a safeguard against potential chromium-related issues, bolstering the overall performance and longevity of the SOEC system.

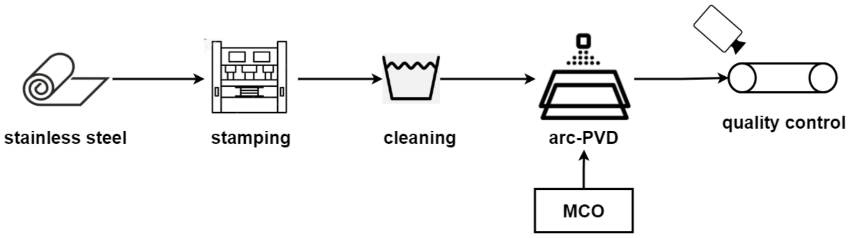

Figure 20: Process flow for interconnect manufacturing

3.2.3 Glass Seal Production Line

Glass seals are essential components in Solid Oxide Electrolyzer Cells (SOECs), fulfilling critical roles in preventing gas mixing and leakage while also providing mechanical stability. The material commonly employed for these seals is BCAS (Barium Calcium Aluminum Silicate), an alkaline earth aluminosilicate glass characterized by its high electrical resistivity, substantial thermal expansion properties, and rapid crystallization kinetics.

In the sealing process, a ball-milled glass paste is carefully applied along the perimeter of the Electrolyte and Electrode Assembly (EEA) cell, serving as the sealing material. This paste ensures a secure and hermetic seal. Subsequently, the EEA cell, now coated with the glass paste, is meticulously positioned onto the frame or substrate, aligning it with precision.

The sealed assembly is then subjected to an annealing process within a furnace. During this controlled heat treatment, a weighted plate is typically positioned above the cell to exert uniform pressure. This annealing step is crucial for achieving a robust and reliable seal.

While cells can be loaded into the annealing furnace in batches, the annealing cycle itself is relatively time-intensive, lasting approximately 330 minutes. This extended duration can be considered a bottleneck in the manufacturing process, potentially affecting production efficiency.

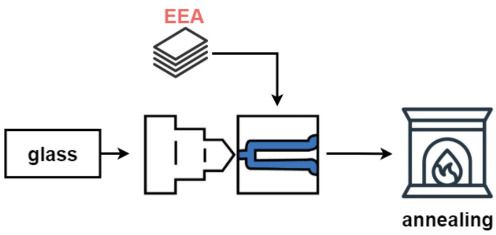

Figure 21: Process flow for glass seal manufacturing

3.2.4 SOEC Assembly Line

In the assembly process bridging the interconnects and EEA cells in Solid Oxide Electrolyzer Cells (SOECs), a pivotal task involves the embedding of glass seals. This embedding operation serves as a critical measure to effectively prevent the occurrence of gas leaks and the unwanted mixing of gases.

The upper segment of Figure 22 portrays a recurrent unit that is to be replicated multiple times, aligning with the specified stack configurations. This repetition is a fundamental requirement for achieving the intended stack configuration and accommodating the desired capacity.

Subsequently, the entire stack, encompassing numerous duplicated units, is subjected to a compression procedure. This compression process can be implemented through either manual labor or automated mechanisms, employing either human workers or robotic systems to apply the necessary pressure.

Throughout the compression phase, additional components such as end plates, compression springs, and various hardware elements are meticulously integrated into the stack assembly. These components are of utmost importance, collectively contributing to the overall structural integrity and operational functionality of the SOEC stack.

In summary, the assembly process entails the embedding of crucial glass seals, the replication of assembly units to meet stack specifications, stack compression for structural stability, and the systematic integration of essential components. This comprehensive procedure ultimately results in the production of a fully functional SOEC stack while avoiding gas leakage and unwanted gas mixing.

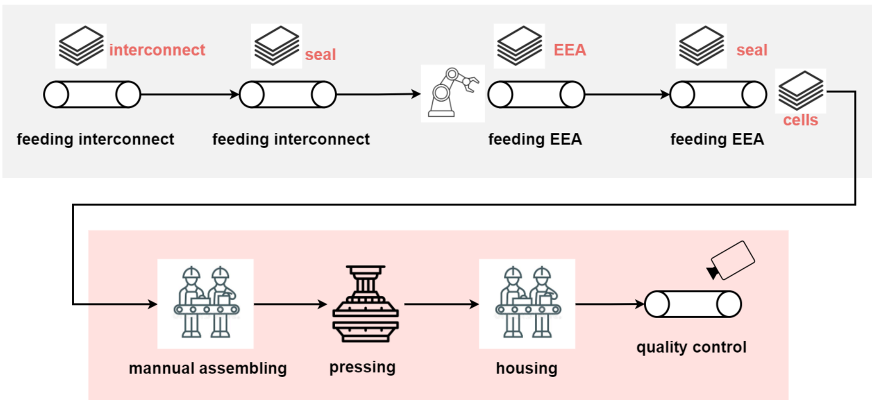

Figure 22: Process flow for SOEC assembly line

4 Results and Conclusions

With the parameters, formulas, and datasets mentioned earlier, we can depict the relationship between unit cost and scale by varying production volumes. The figure below illustrates a significant decrease in manufacturing costs. Starting from a production volume of 100 MW/y and increasing to 1000 MW/y, the unit cost for PEMEC drops from 184.5 \$/kW to 96.6 \$/kW, while SOEC costs decrease from 155.8 \$/kW to 68.6 \$/kW.

As evident from the figure, costs decrease rapidly when production volumes are below 500 MW/y, primarily due to the establishment of an exponential correlation between cost and volume. However, once production exceeds 500 MW/y, this reduction rate slows down because the prices of certain materials reach their minimum values and cease to decrease with increasing volume. Instead, the reductions in non-material costs, such as labor and capital, become the dominant factors affecting the total costs.

Furthermore, in the range where the volume exceeds 10,000 MW/y, the cost remains nearly constant, approaching the minimum marginal cost. The marginal cost represents the change in total cost that occurs when the quantity produced is increased – in other words, it is the cost of producing an additional quantity[26].

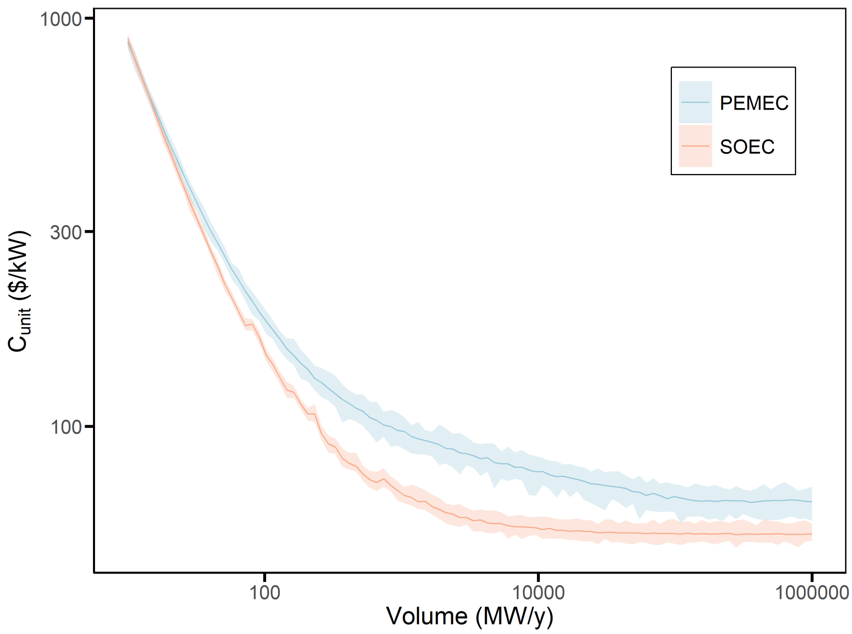

Figure 23: Cost evolution of PEMEC and SOEC with annual production volume

In the context of environmental impact assessment, we have chosen to focus on the carbon footprint as an illustrative example to elucidate the implications of scale effects. Notably, the carbon footprint exhibits a distinct pattern characterized by a steep initial decline followed by a subsequent flattening. This pattern is more precisely elucidated in the figure.

Specifically, when transitioning from a production volume of 100 MW/y to 1000 MW/y, we observe a reduction in the carbon footprint per PEM system from 40,702.4 kg/system to 40,429.3 kg/system.

Conversely, for SOEC systems, the carbon footprint per unit decreases from 4,207.9 kg/system to 3,384.6 kg/system over the same scale-up range.

These findings accentuate the pronounced influence of scale on the carbon footprint. The steep initial decrease signifies the efficiency enhancements attributed to the scaling effect, where fixed environmental costs are dispersed over a greater production volume. This underscores the need to assess the ideal production volume, considering both economic and environmental viewpoints. However, the ensuing plateau in the trend implies that beyond a particular threshold, material consumption becomes the chief driver of the overall carbon footprint.

As indicated by the data, the utilization of precious metals like platinum and gold contributes to this outcome. This revelation serves as an impetus for exploring alternative materials that are more environmentally sustainable.

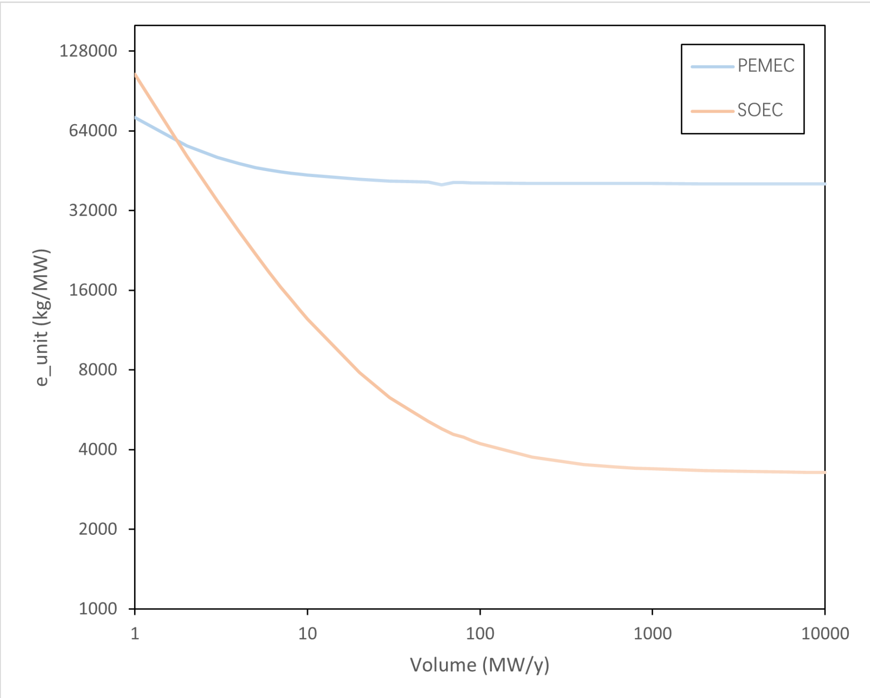

Figure 24: Environmental impacts evolution of PEMEC and SOEC with annual production volume

In Figure 26, stacked bar charts are presented illustrating the capital and maintenance costs associated with PEMEC and SOEC technologies at different production volumes, specifically 100 MW/y and 1000 MW/y. Notably, a significant reduction in costs is observed as production volume scales up, owing to the amortization of capital expenses across a larger number of units. Concurrently, material costs exhibit a sharp decline.

Of particular interest is the cost breakdown of the Catalyst Coated Membrane (CCM), a critical component of PEMEC. At the 100 MW/y production volume, CCM accounts for approximately 40% of the total cost, rising to 56% at the 1000 MW/y volume. It is noteworthy that the material cost of CCM is a substantial contributor, constituting around 80% of the total cost due to the use of noble metals in catalyst ink. This underscores the pressing challenge of minimizing noble metal usage in CCM to achieve cost reductions.

Additionally, the material costs associated with the Proton-Exchange Membrane (PTL) and bipolar plates become increasingly significant at higher production volumes, as non-material costs proportionally decrease. Notably, our findings reveal that the carbon coating used in cathode PTL incurs higher costs compared to sintered titanium felts employed in anode PTL, which are produced in-house. Consequently, exploring alternatives such as replacing carbon cloth with titanium felts or more cost-effective porous materials appears to be a promising avenue for cost reduction.

Turning our attention to assembly and frame processes, labor costs emerge as the predominant factor. Implementing novel techniques or automated production lines represents an economically viable strategy for simultaneously curbing capital costs and labor expenditures. However, it is worth noting that, relative to other cost components, the expenses associated with these two aspects are relatively minor. Consequently, it may be prudent to allocate fewer resources towards their improvement at this juncture.

In conclusion, our analysis underscores the critical importance of optimizing various cost elements in the production of PEMEC and SOEC systems. While the amortization of capital expenses and reduction of noble metal usage in CCM are primary avenues for cost reduction, exploring alternative materials for PTL and bipolar plates, as well as enhancing production processes, can further enhance cost-efficiency in large-scale manufacturing.

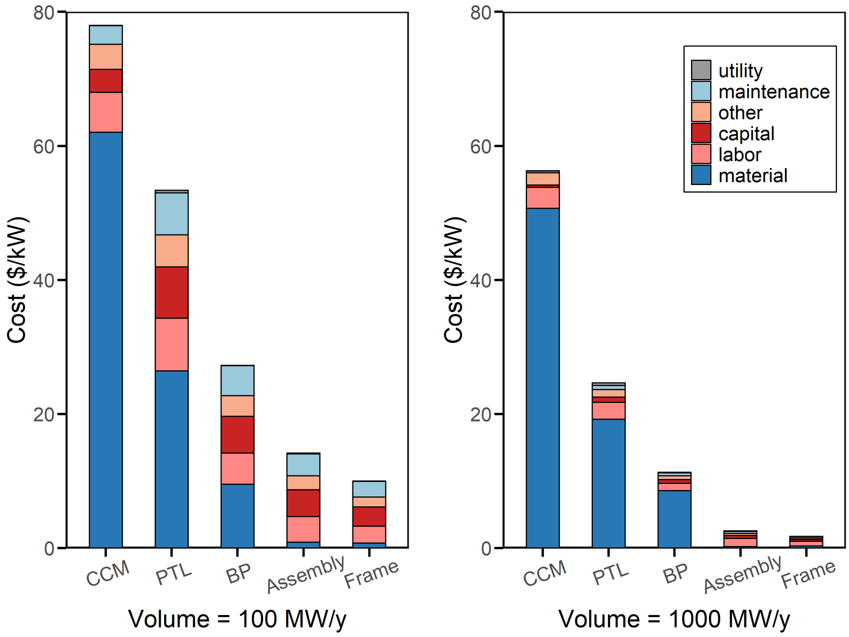

Figure 25: Cost components of PEMEC at an annual production volume of 100 MW/y and 1000 MW/y

In an examination of the carbon footprints of PEM (Proton Exchange Membrane) systems, particularly at annual production volumes of 100 MW/y and 1000 MW/y, a notable trend emerges. The aggregate carbon emissions appear to stabilize at approximately 40,000 kg of carbon dioxide per system. It is worth noting that the contributions of infrastructure and equipment to the carbon footprint are relatively diminutive, and energy-related emissions are comparably negligible when juxtaposed with emissions stemming from material use.

In contradistinction to financial analysis, where cost is the focal point, the substantial carbon dioxide emissions associated with the extensive use of rare materials, such as platinum, titanium, and gold, though characterized by low consumption levels, can be primarily attributed to their high Global Warming Potential (GWP) factor. This underscores the salience of materials as the principal determinant of the elevated carbon footprint throughout various phases of the production process.

In summation, this outcome underscores a compelling avenue for the reduction of carbon dioxide emissions within the purview of hydrogen gas production technology: the exploration and incorporation of alternative materials. This approach holds significant potential for mitigating the environmental ramifications tied to the utilization of rare materials with elevated GWP values, all without necessitating fundamental alterations to the underlying hydrogen production methodologies.

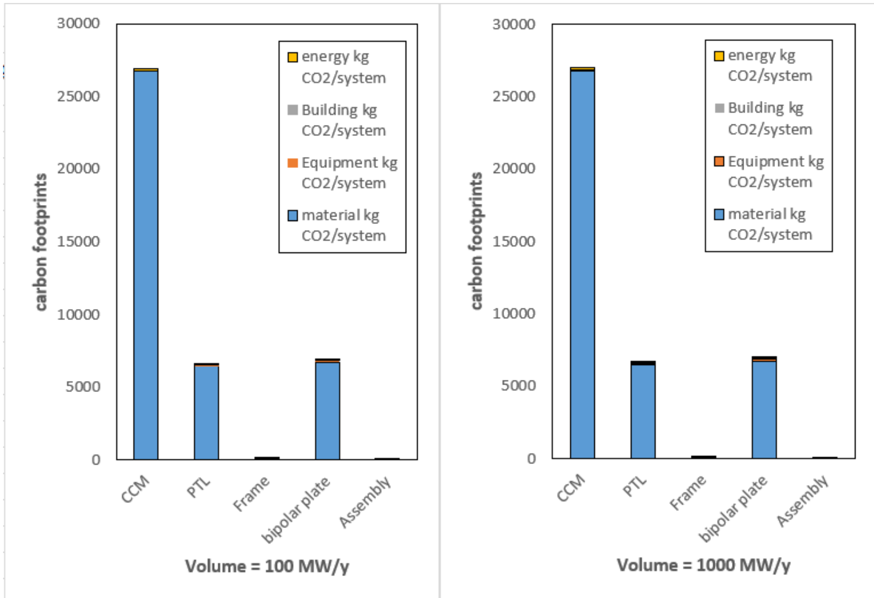

Figure 26: Carbon footprint components of PEMEC at an annual production volume of 100 MW/y and 1000 MW/y

In contrast to PEMEC, the cost breakdown for SOEC reveals distinct characteristics, with material costs representing a notably smaller proportion (less than 25%) of the total cost. Labor costs emerge as the primary cost contributor, followed closely by capital costs. Therefore, it is advisable to explore avenues for increasing automation levels or implementing novel techniques in SOEC production facilities to mitigate overall costs.

Remarkably, the production of SOEC demonstrates more pronounced economies of scale (EoS) compared to PEMEC. This can be attributed to the smaller share of material costs in the overall cost structure. However, it's important to note that there is a limit to cost reduction associated with manufacturing, primarily determined by the minimum attainable material cost. Beyond this point, cost reduction is primarily driven by decreases in non-material costs as production volume increases.

Based on our analysis, the lowest achievable cost for PEMEC is approximately 65$perkilowatt$(/kW), while for SOEC, it stands at approximately 52/kW. The reduction in costs initially hinges on significant reductions in material prices or capital costs, which are inherently tied to the proportional contribution of each component to the total cost. However, once this limit is reached, only the non-material costs continue to decrease as production volume expands.

Consequently, it is evident that regardless of the extent of plant expansion, the cost of PEMEC consistently exceeds that of SOEC, primarily due to its higher material cost, which remains a significant cost driver even at larger production scales.

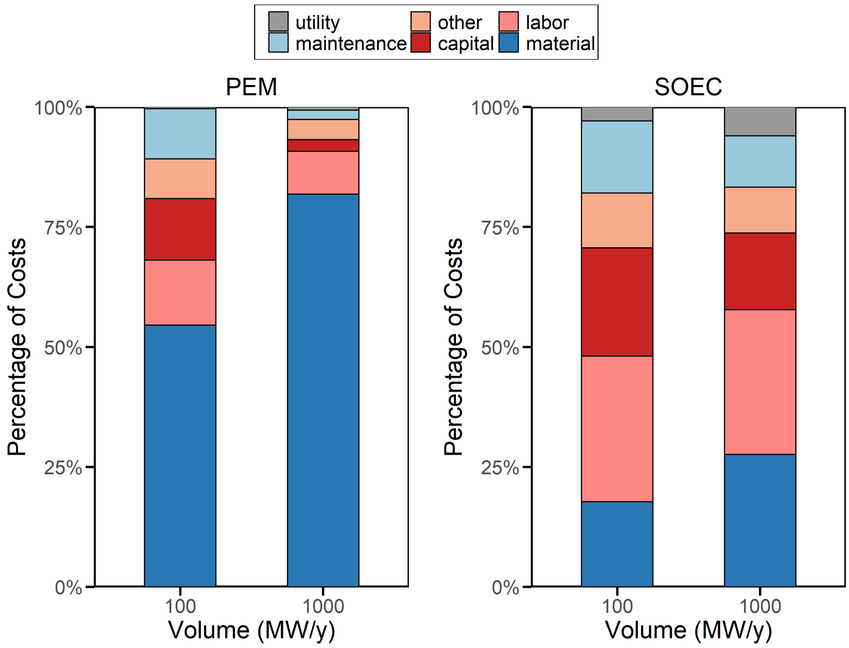

Figure 27: Cost components of PEMEC and SOEC at annual production volume of 100 MW/y and 1000 MW/y

Comparable to the distinctions observed between PEM (Proton Exchange Membrane) and SOEC (Solid Oxide Electrolysis Cell), the differentiation among individual sections within PEM is less conspicuous, primarily due to the overriding influence of materials, as elucidated earlier. In the case of SOEC, the carbon footprints originating from materials constitute a smaller proportion of the total footprint, approximating around 30%. The pivotal factor here is the substantial contribution of energy, which serves as a catalyst for encouraging the exploration of more environmentally sustainable energy generation methods.

Furthermore, it is discernible that the scale effect in SOEC exhibits a more pronounced manifestation than in PEM. With the augmentation of annual production, the relative allocations for construction and equipment consistently diminish. Simultaneously, energy and material become the predominant contributors to carbon dioxide emissions. Nevertheless, it is important to acknowledge that the carbon footprint possesses a lower limit, which is dictated by the combined direct contributions of material and energy. Prior to reaching this threshold, the marginal carbon footprint comprises indirect contributions emanating from infrastructure and equipment.

Building upon the aforementioned empirical data and synthesizing it with subsequent insights, it becomes evident that the annual carbon footprints of SOEC are higher than those of PEM up until annual production exceeds 3 MW, a scenario that is unrealistic in practical terms. Consequently, regardless of the scale magnitude, SOEC maintains a lower Global Warming Potential (GWP) in comparison to PEMEC. This observation aligns with the conclusion derived from cost analysis, underscoring the pivotal role of material selection as the principal determinant behind this discrepancy.

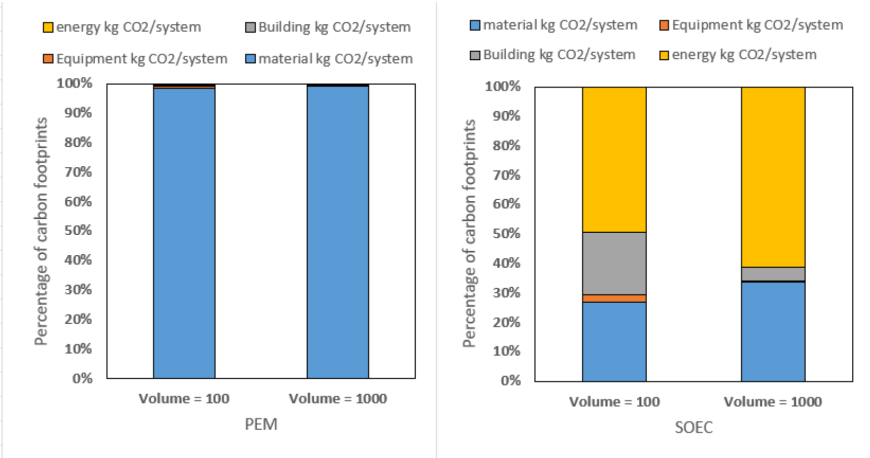

Figure 28: CO2 components of PEMEC and SOEC at an annual production volume of 100 MW/y and 1000 MW/y

As illustrated in Figure 30, the distribution of total costs within SOEC exhibits a more balanced allocation across its various components compared to PEMEC. In both production scenarios, labor and capital costs stand out prominently as the primary cost components, even though they experience substantial reductions when scaling production from 100 MW/y to 1000 MW/y. This observation underscores the need for the adoption of advanced and labor-saving technologies in the manufacturing processes of SOEC.

Furthermore, in pursuit of cost efficiency and to spread the costs across a greater number of units, producers of SOEC systems would be well-advised to continue increasing production volumes. This strategy aligns with the economies of scale principle, where larger production quantities can help distribute fixed costs more effectively, ultimately leading to cost savings.

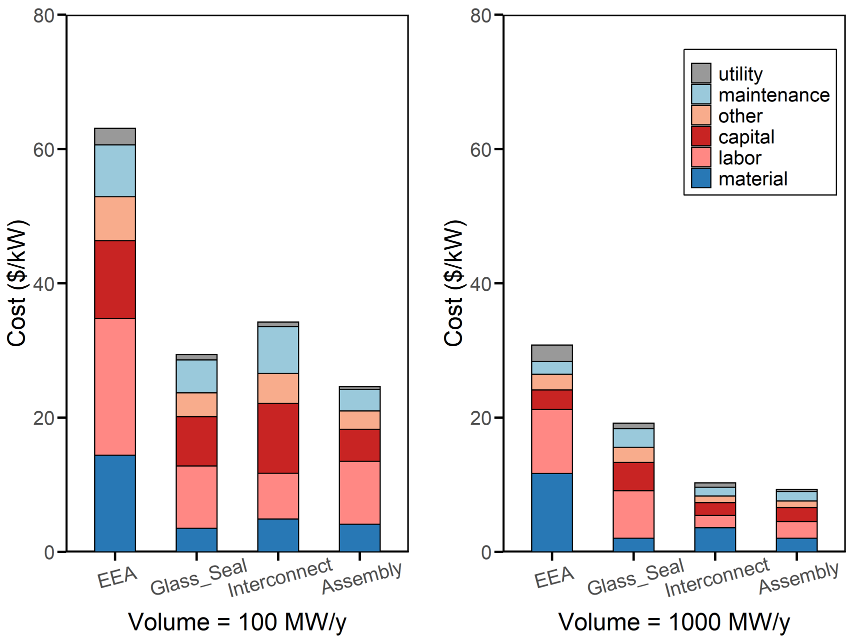

Figure 29: Cost components of SOEC at an annual production volume of 100 MW/y and 1000 MW/y

As depicted in the subsequent figure, in comparison to PEMEC, the distribution of total carbon footprints across each production section exhibits a more equitable allocation. However, it remains apparent that energy and materials continue to be the principal contributors to carbon dioxide emissions, with indirect contributions also maintaining significance, albeit diminishing as annual production scales upward.

In conclusion, the adoption of low-carbon energy sources emerges as a pivotal strategy for mitigating the overall carbon footprint. Simultaneously, enhancements in infrastructure design and technological pathways bear substantial potential to curtail carbon dioxide emissions. Future research endeavors should prioritize these focal points for comprehensive analysis and improvement.

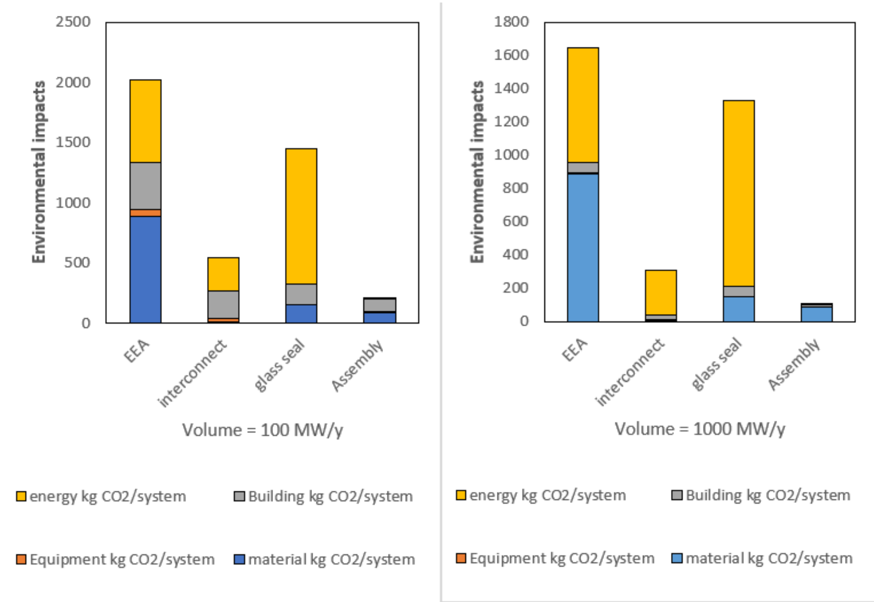

Figure 30: Cost components of SOEC at an annual production volume of 100 MW/y and 1000 MW/y

5 Discussion

The primary objective of this bottom-up modeling endeavor is to undertake a comprehensive assessment of two distinct hydrogen production equipment technologies. This assessment encompasses the estimation of their future cost trajectories and the analysis of their corresponding environmental impacts. These estimations are rooted in data derived from the International Energy Agency (IEA) and are presented as follows:

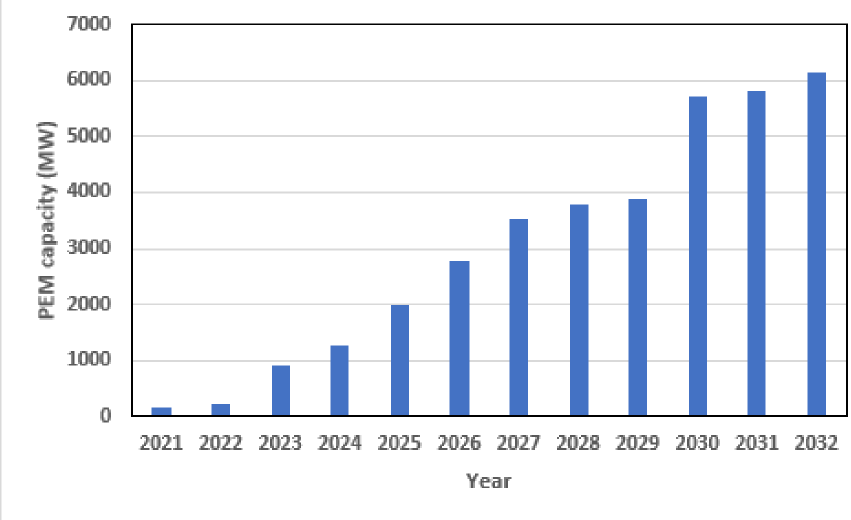

Figure 31: Global PEM annual installed capacity changes with the year

Expanding upon the previous figures, it is evident that the unit cost of PEM (Proton Exchange Membrane) technology can be estimated by considering the installation quantity of PEM units, as illustrated in the subsequent figure. The figure demonstrates a notable trend wherein the unit cost is projected to stabilize at approximately \$420 per kilowatt (kW) in the foreseeable future. This level represents a noteworthy reduction in costs when juxtaposed with the current expenses associated with PEM technology.

This trend underscores the potential for significant cost optimization and increased economic feasibility in the deployment of PEM technology. The projected stabilization of unit costs at this relatively low level indicates a promising outlook for the affordability and scalability of PEM-based hydrogen production in the coming years.

This analysis relies on the empirical data and figures at hand, providing valuable insights into the cost dynamics of PEM technology and its potential for cost-effective hydrogen production in the future.

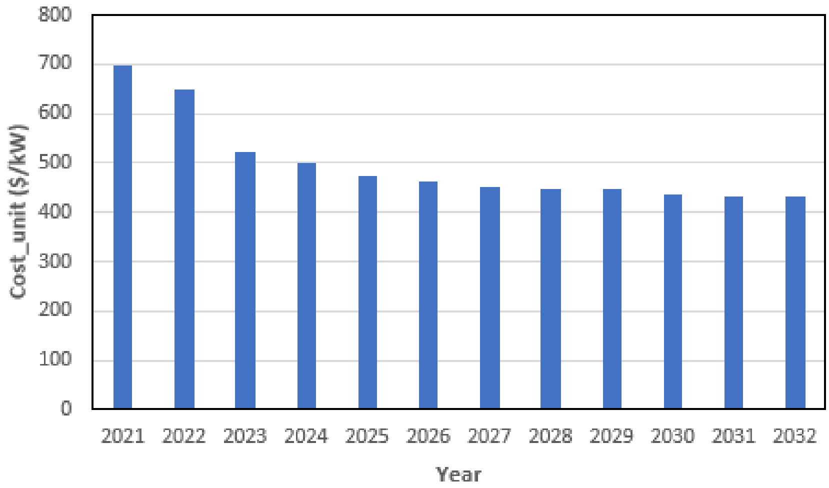

Figure 32: PEM unit cost estimation with the year

In the realm of environmental impact assessment, our model parallels its role in cost analysis, thereby furnishing a comprehensive and intricately detailed evaluation applicable to the foreseeable future. A distinctive trend identified within this framework is the inverse correlation between environmental impacts and the augmentation of production scale, where a notable reduction in environmental repercussions is observed with an expansion in scale. It is imperative to underline that these discerned conclusions and analytical methodologies are extensible and germane to a broader spectrum of industries.

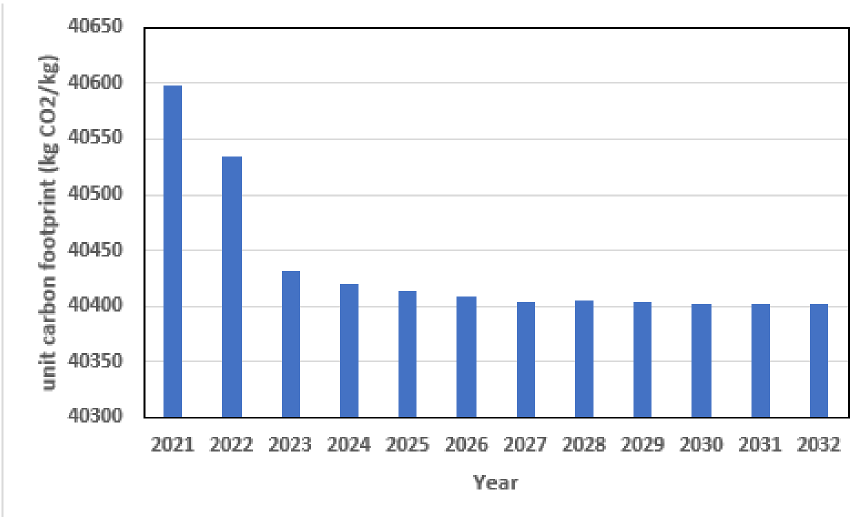

Figure 33: PEM unit carbon footprint evaluation with the year

Correspondingly, SOEC has similar analysis originating from its production within recent years, here are the figures.

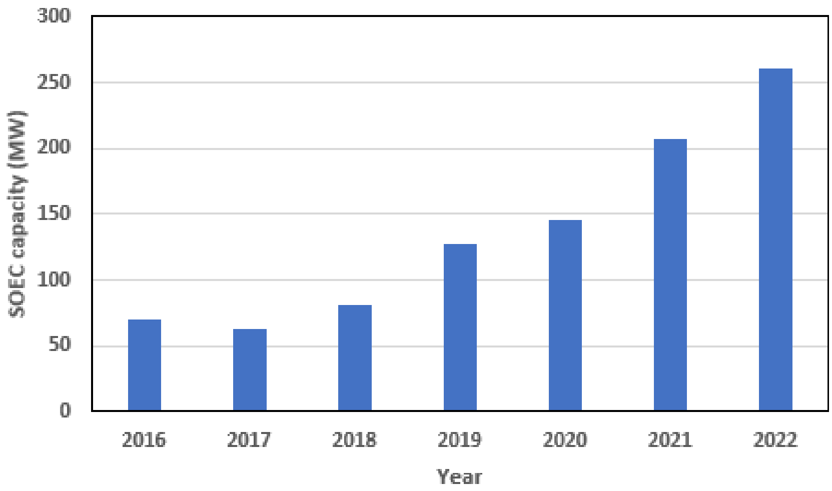

Figure 34: Global SOEC annual installed capacity changes with the year

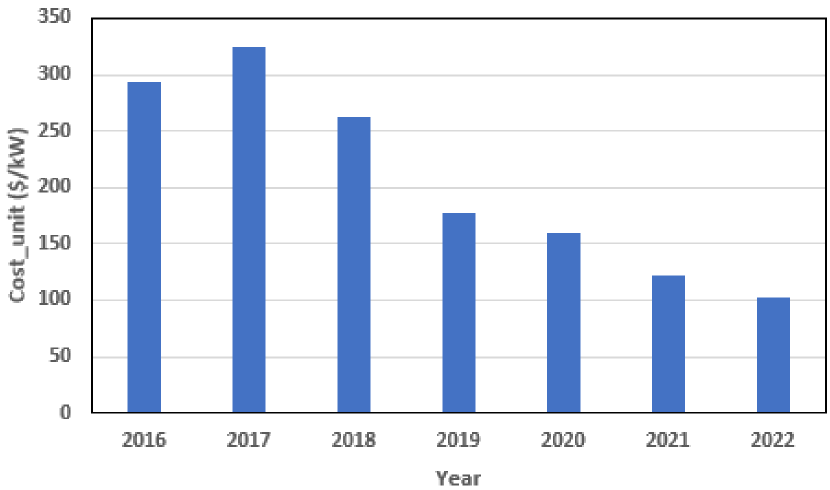

Figure 35: SOEC unit cost estimation with the year

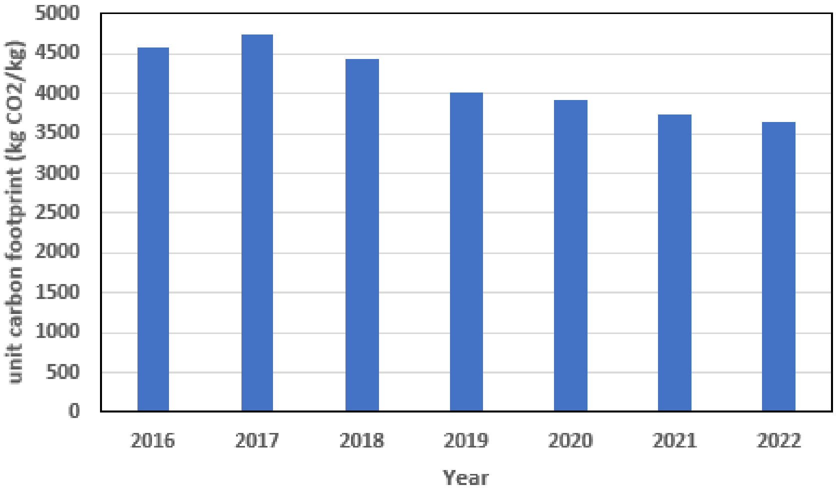

Figure 36: SOEC unit carbon footprint evaluation with the year

Within this context, the dynamics of environmental impacts as they relate to production scale in hydrogen production, and by extension, other industries, can be elucidated as follows:

1. **Scale-Induced Efficiencies:** As production scale amplifies, a salient effect emerges in the form of economies of scale. This effect precipitates a reduction in environmental impacts per unit of output. This diminishment is explicable by enhanced operational efficiencies, the adept utilization of resources, and the concomitant decline in emissions intensity. For instance, within the domain of hydrogen production, a larger-scale facility could realize economies of scale leading to a diminished environmental footprint per unit of hydrogen generated.

2. **Technological Progression:** The inexorable march of technological advancement exerts a pivotal influence on environmental implications. Emerging technologies invariably proffer augmented efficiency and mitigated environmental footprints. Such technological innovation, underpinned by research and development endeavors, contributes substantively to the observed abatement in environmental impacts with an expanded production scale.

3. **Resource Optimization:** The stewardship of resources assumes heightened significance with an escalation in production scale. Larger-scale production facilities oftentimes institute sophisticated resource management practices, encompassing the deployment of energy-efficient equipment, the systematic recycling of materials, and the concomitant curtailment of waste generation. These practices collectively conduce to a discernible reduction in environmental burdens.

4. **Regulatory and Ethical Imperatives:** The elevation of production scale may instigate the enactment of more stringent environmental regulations and an augmented sense of corporate environmental responsibility. The resultant impact encompasses an intensified commitment to proactively diminish and ameliorate environmental impacts.

5. **Lifecycle Analysis:** Holistic environmental assessments incorporate a comprehensive evaluation of the entire lifecycle of a product or process. Such assessments span the spectrum from the extraction of raw materials to production, distribution, and ultimate disposal or recycling. As production scales up, opportunities arise for the optimization of various lifecycle stages,

which, in tandem, yield an overarching diminishment in environmental impacts.

6. **Sustainability Reporting:** Prevailing trends in contemporary industry underscore the imperative of sustainability reporting. A larger production scale is frequently concomitant with an augmented impetus for entities to systematically measure, report, and diminish their environmental impacts. This arises from the exigencies of satisfying stakeholder expectations and aligning with evolving regulatory frameworks.

It is thus evident that the identified conclusions and analytical paradigms, which manifest acutely within the context of hydrogen production, are amenable to generalization and applicability across a diverse array of industries. This serves as a beacon for prudent decision-making, propounding the viability of strategic scaling, pioneering innovations, and the judicious exercise of environmental stewardship as avenues towards the realization of sustainability objectives.

6 Conclusion

With the utilization of the bottom-up model, we have effectively addressed the intricate relationships between cost, environmental impact, and annual production volumes, providing a comprehensive understanding of the mechanisms governing Economies of Scale (EoS) and Life Cycle Assessment(LCA). However, it is crucial to acknowledge that due to limited information from vendors or industry experts, we have had to rely on several assumptions to estimate costs. Therefore, further endeavors are warranted to gather precise parameters from vendors or conduct a more extensive review of the existing literature.

Moreover, to enhance the accuracy of assessing manufacturing costs and environmental impacts at specific points in time, we can integrate the model with online databases to directly access real-time material prices. Additionally, the classification of cost components can be refined, with the material cost, capital cost, and other factors being delineated more explicitly. This refined approach can yield a more precise EoS curve.

In this paper, we have primarily considered the variability in material prices as well as their environmental impacts, with the fluctuations in other parameters being disregarded. However, it is imperative to conduct a comprehensive error analysis, accounting for all potential sources of variability and uncertainty.

Indeed, the overarching objective of this research is to elucidate the learning effect. We recognize that this can be achieved by incorporating additional elements into the model, such as Learning-by-Doing (LBD), advancements in manufacturing techniques, and evolving technologies. For instance, LBD can be evaluated through the analysis of variance in scrap rates with varying production volumes. By progressively enhancing the current model, we can develop its capacity to effectively characterize the learning effect.

Furthermore, this model possesses the inherent potential to adapt to diverse industrial processes by parameter substitution. It can subsequently be harnessed to decipher the learning effects associated with numerous emerging techniques, facilitating cost predictions. These predictions, in turn, provide invaluable guidance for both researchers and investors in their pursuit of innovation and efficiency within various industries.

References

[1] "Hydrogen," IEA. (2021), [Online]. Available: https://www.iea.org/reports/hydrogen (visited on 09/01/2022).

[2] A. M. Elshurafa, S. R. Albardi, S. Bigerna, and C. A. Bollino, "Estimating the learning curve of solar PV balance–of–system for over 20 countries: Implications and policy recommendations," *Journal of Cleaner Production*, vol. 196, pp. 122–134, Sep. 20, 2018. [Online]. Available: https://www.sciencedirect.com/science/article/pii/S0959652618316652 (visited on 08/30/2022).

[3] A. J. C. Trappey, C. V. Trappey, H. Tan, P. H. Y. Liu, S.-J. Li, and L.-C. Lin, "The determinants of photovoltaic system costs: An evaluation using a hierarchical learning curve model," *Journal of Cleaner Production*, Preventing Smog Crises, vol. 112, pp. 1709–1716, Jan. 20, 2016. [Online]. Available: https://www.sciencedirect.com/science/article/pii/S0959652615011968 (visited on 09/01/2022).

[4] S. Lu, Ed., *Economies of Scale in PEMEC and SOEC Manufacturing based on a Bottom-up Model*. 2022.

[5] J. B. Guinée, H. A. Udo de Haes, and G. Huppes, "Quantitative life cycle assessment of products: 1:Goal definition and inventory," *Journal of Cleaner Production*, vol. 1, no. 1, pp. 3–13, Jan. 1993. [Online]. Available: https://www.sciencedirect.com/science/article/pii/0959652693900279 (visited on 08/24/2023).

[6] A. Jørgensen, A. Le Bocq, L. Nazarkina, and M. Hauschild, "Methodologies for social life cycle assessment," en, *The International Journal of Life Cycle Assessment*, vol. 13, no. 2, pp. 96–103, Mar. 2008. [Online]. Available: https://doi.org/10.1065/lca2007.11.367 (visited on 08/24/2023).

[7] O. Schmidt, A. Gambhir, I. Staffell, A. Hawkes, J. Nelson, and S. Few, "Future cost and performance of water electrolysis: An expert elicitation study," en, *International Journal of Hydrogen Energy*, vol. 42, no. 52, pp. 30 470–30 492, Dec. 2017. [Online]. Available: https://www.sciencedirect.com/science/article/pii/S0360319917339435 (visited on 04/03/2022).

[8] M. van Amsterdam, "Factorial techniques applied in chemical plant cost estimation: A comparative study based on literature and cases," M.S. thesis, Delft University of Technology, 2018.

[9] M. S. Peters, K. D. Timmerhaus, and R. E. West, *Plant design and economics for chemical engineers*. New York: McGraw-Hill Professional, 2002.

[10] U. D. of Energy, "Engineering economic analysis guide: Liquid fuels technologies," U.S. Energy Information Administration, Tech. Rep., 2015.

[11] B. Cheng, K. Lu, J. Li, H. Chen, X. Luo, and M. Shafique, "Comprehensive assessment of embodied environmental impacts of buildings using normalized environmental impact factors," en, *Journal of Cleaner Production*, vol. 334, p. 130 083, Feb. 2022, JCR: Q1 : 1 : 11.1 5: 11.0 EI:. [Online]. Available: https://linkinghub.elsevier.com/retrieve/pii/S0959652621042499 (visited on 07/12/2023).

[12] C. K. Anand and B. Amor, "Recent developments, future challenges and new research directions in LCA of buildings: A critical review," en, *Renewable and Sustainable Energy Reviews*, vol. 67, pp. 408–416, Jan. 2017, JCR: Q1 : 1 : 15.9 5: 16.9 EI:. [Online]. Available: https://linkinghub.elsevier.com/retrieve/pii/S1364032116305524 (visited on 07/12/2023).

[13] P. A. Nelson, S. Ahmed, K. G. Gallagher, and D. W. Dees, "Modeling the performance and

cost of lithium-ion batteries for electric-drive vehicles, third edition," Mar. 2019. [Online]. Available: `https://www.osti.gov/biblio/1503280`.

[14] "Public announcement of the environmental assessment report on hydrogen production plant with an annual capacity of 120 units (sets)," Suzhou Wanshun Hydrogen Energy Technology, Tech. Rep., 2019.

[15] "Environmental impact report form for pem equipment rd platform project," Sungrow Power Supply, Tech. Rep., 2020.

[16] L. Middelhauve, j. Granacher, and M. François, "Cost estimation of a technology," École Polytechnique Fédérale de Lausanne, Tech. Rep., 2021.

[17] R. Scataglini, A. Mayyas, M. Wei, *et al.*, "A Total Cost of Ownership Model for Solid Oxide Fuel Cells in Combined Heat and Power and Power-Only Applications," en,

[18] R. Scataglini, M. Wei, A. Mayyas, S. H. Chan, T. Lipman, and M. Santarelli, "A direct manufacturing cost model for solid-oxide fuel cell stacks," *Fuel Cells*, vol. 17, no. 6, pp. 825–842, Dec. 2017. [Online]. Available: `https://onlinelibrary.wiley.com/doi/10.1002/fuce.201700012` (visited on 07/28/2022).

[19] R. D. Stewart, R. M. Wyskida, and J. D. Johannes, *Cost Estimator's Reference Manual.* New Jersey: Wiley, 1995.

[20] W. Grubb and L. Niedrach, "Batteries with solid ion-exchange membrane electrolytes: II. low-temperature hydrogen-oxygen fuel cells," *Journal of the Electrochemical Society*, vol. 107, no. 2, pp. 131–135, 1960.

[21] C. I. Morfopoulou, A. K. Andreopoulou, M. K. Daletou, S. G. Neophytides, and J. K. Kallitsis, "Cross-linked high temperature polymer electrolytes through oxadiazole bond formation and their applications in HT PEM fuel cells," *Journal of Materials Chemistry A*, vol. 1, no. 5, pp. 1613–1622, 2013, Publisher: Royal Society of Chemistry. [Online]. Available: `https://pubs.rsc.org/en/content/articlelanding/2013/ta/c2ta00610c` (visited on 08/25/2022).

[22] A. T. Mayyas, M. F. Ruth, B. S. Pivovar, G. Bender, and K. B. Wipke, "Manufacturing Cost Analysis for Proton Exchange Membrane Water Electrolyzers," en, Tech. Rep. NREL/TP-6A20-72740, 1557965, Aug. 2019, NREL/TP–6A20–72 740, 1 557 965. [Online]. Available: `http://www.osti.gov/servlets/purl/1557965/` (visited on 01/01/2022).

[23] W. Dönitz and E. Erdle, "High-temperature electrolysis of water vapor—status of development and perspectives for application," *International Journal of Hydrogen Energy*, vol. 10, no. 5, pp. 291–295, Jan. 1, 1985. [Online]. Available: `https://www.sciencedirect.com/science/article/pii/0360319985901818` (visited on 08/25/2022).

[24] R. Anghilante, D. Colomar, A. Brisse, and M. Marrony, "Bottom-up cost evaluation of SOEC systems in the range of 10–100 MW," *International Journal of Hydrogen Energy*, vol. 43, no. 45, pp. 20 309–20 322, Nov. 8, 2018. [Online]. Available: `https://www.sciencedirect.com/science/article/pii/S0360319918327368` (visited on 06/21/2022).

[25] F. M. Sapountzi, J. M. Gracia, C. J. Weststrate, H. O. A. Fredriksson, and J. W. Niemantsverdriet, "Electrocatalysts for the generation of hydrogen, oxygen and synthesis gas," *Progress in Energy and Combustion Science*, vol. 58, pp. 1–35, Jan. 1, 2017. [Online]. Available: `https://www.sciencedirect.com/science/article/pii/S0360128516300260` (visited on 08/24/2022).

[26] A. O'Sullivan, S. M. Sheffrin, i. Prentice-Hall, and Wall Street Journal (Firm), *Economics : principles in action*, in collab. with Library Genesis. Needham, Mass. : Prentice Hall, 2003, 609 pp. [Online]. Available: `http://archive.org/details/economicsprincip00osul` (visited on 08/28/2022).

A Appendix

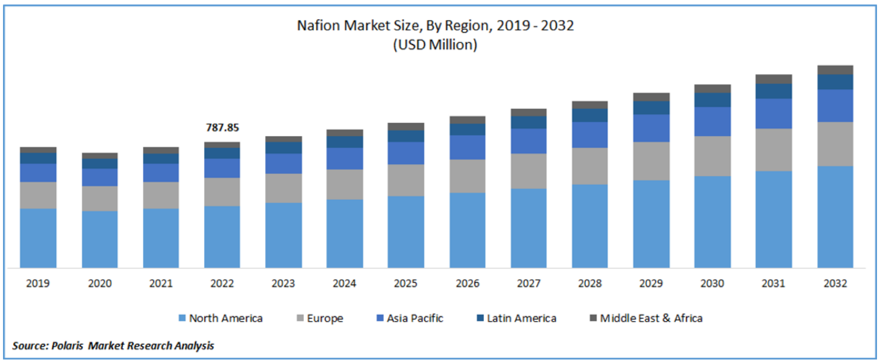

Figure 37: nafion market size

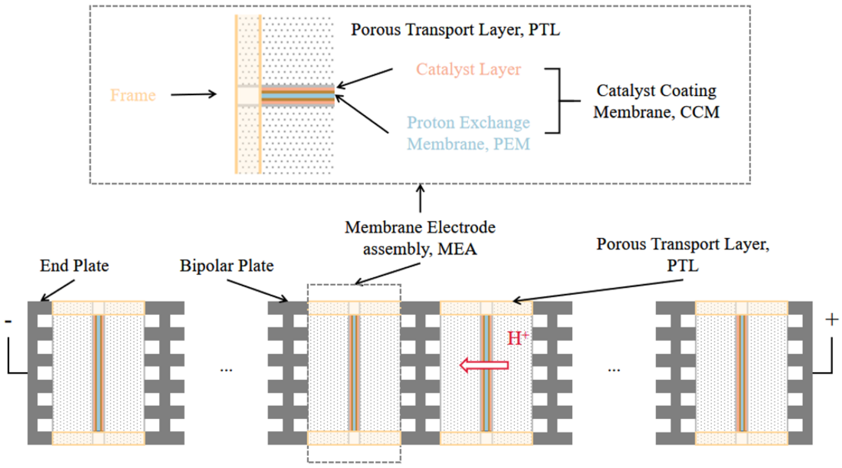

Figure 38: PEM structure

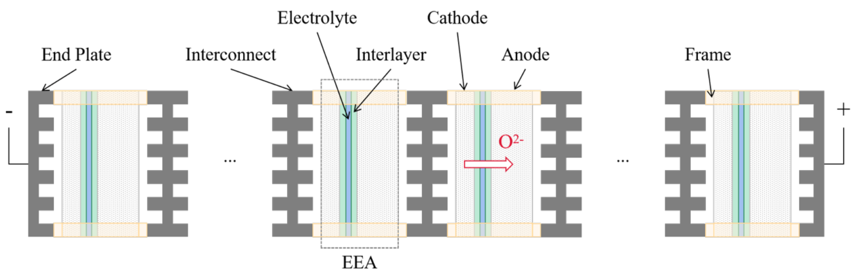

Figure 39: structure of SOEC, Scataglini, R., M. Wei, A. Mayyas, S. H. Chan, T. Lipman, and M. Santarelli, Fuel Cells, 2017.

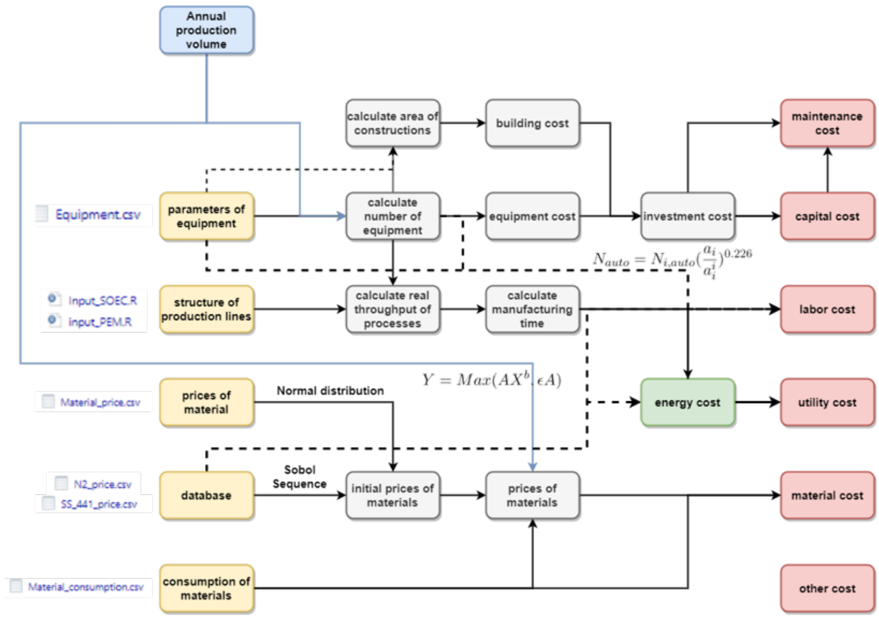

Figure 40: cost model

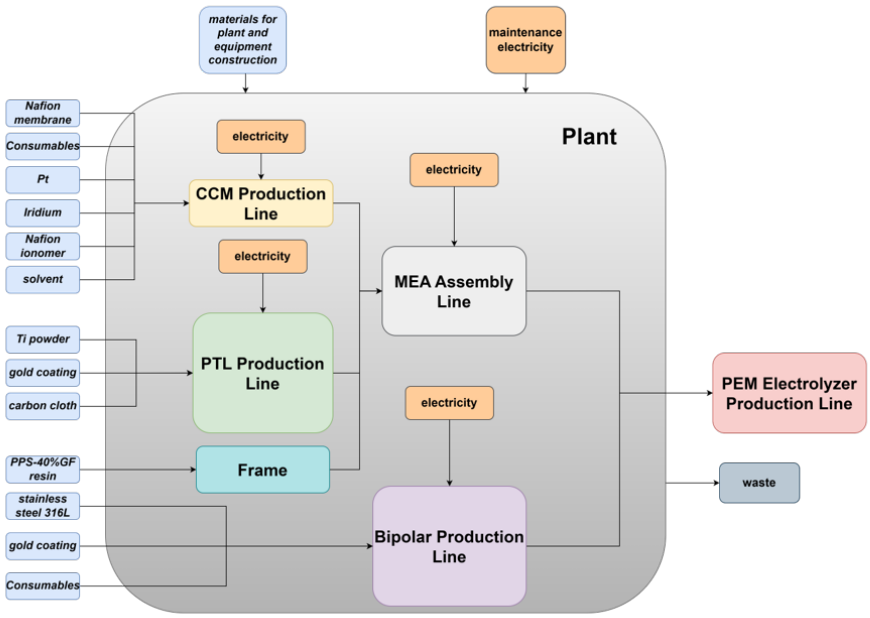

Figure 41: boundary system

Quality level I: recommended and satisfactory	*Quality level II: recommended, some improvements needed*	*Quality level III: recommended, but to apply with caution*
Climate change	***Acidification, terrestrial and freshwater***	***Land use***
Ozone depletion	***Eutrophication, fresh water, terrestrial and marine***	***Water scarcity***
Particulate depletion	***Ionizing radiation***	***Resource depletion, fossil, and mineral and metal0***
	Photochemical ozone formation	
	Human toxicity, cancer and non-cancer effects(II/III)	
	Ecotoxicity, freshwater(II/III)	

Figure 42: EI matrix

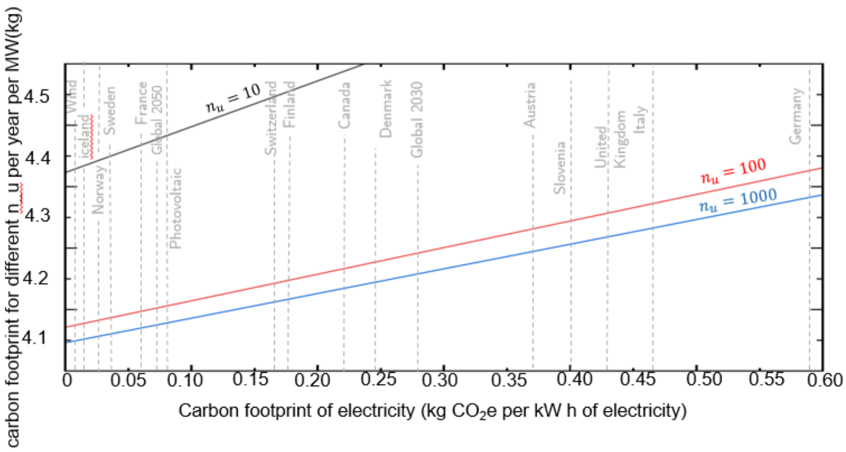

Figure 43: carbon footprints change with electricity carbon footprints evolution

CCM	material used: kg							
	steel	aluminium	copper	others	weight	area	power kW	price $
cleaning	5895.6	0.0	310.3	0.0	6,206	1.0668	8.25	6952.85
drying	1500.0	300.0	300.0	308.0	2,400	9.46	54	11120.64
mixing	5895.6	0.0	310.3	0.0	6,206	1.0668	8.25	6952.85
deforming	902.5	0.0	47.5	0.0	950	0.936	25	8343.53
quarlity control	/							
spraying	455.0	97.5	65.0	32.5	650	1.24	80	6536.86
drying	1500.0	300.0	300.0	308.0	2,400	9.46	54	11120.64
mixing	5895.6	0.0	310.3	0.0	6,206	1.0668	8.25	6952.85
deforming	902.5	0.0	47.5	0.0	950	0.936	25	8343.53
spraying	455.0	97.5	65.0	32.5	650	1.24	80	9455.87
quarlity control	/							
cutting	500.0	400.0	45.0	0.0	945	4	9	4171.71
PTL								
	steel	aluminium	copper	others		area		price $
mixing	5895.6	0.0	310.3	0.0	6,206	1.0668	8.25	6952.85
compacting	1750.0	375.0	125.0	250.0	2,500	6.63	4	6000
sintering	204.1	31.4	15.7	62.8	314	2.7813	6	27811.77
PVD coating	480.0	240.0	120.0	360.0	1,200	0.378	5	68000
quarlity control	/							
cutting	500.0	400.0	45.0	0.0	945	4	9	4171.71
MEA								
	steel	aluminium	copper	others		area		price $
injection molding	24.0	8.0	4.0	4.0	40	12.2412	40	11124.4
BP								
	steel	aluminium	copper	others		area		price$
blanking	1800.0	600.0	300.0	300.0	3000	7.5425	4.5	21000
stamping	10800.0	3600.0	1800.0	1800.0	18000	27.18	46	111242.48
cleaning	5895.6	0.0	310.3	0.0	6,206	1.0668	8.25	6952.85
PVD coating	480.0	240.0	120.0	360.0	1200	0.378	5	68000
quality control								
assembly								
	steel	aluminium	copper	others		area		price$
feeding bipolar plate								
print gasket	396.0	132.0	66.0	66.0	660	1.7696	2.75	6674.55
UV curing	180.0	60.0	30.0	30.0	300	5.152	16	9717.9
adding MEA								
print gasket	396.0	132.0	66.0	66.0	660	1.7696	2.75	6674.55
UV curing	180.0	60.0	30.0	30.0	300	5.152	16	9717.9

EEA	steel				rubber	Ti	ceramic
slurry mixer	5895.6		310.3				
ball mill	55	11	11				
de-airing	296.82		16.49				
tape casting							
drying	1500	300	300	300	8		
quality control							
peeling							
slurry mixer	5895.6		310.3				
screen painting	396	132	66				
drying	1500	300	300	300	8		
slurry mixer	5895.6		310.3				
screen printing	396	132	66				
drying	1500	300	300	300	8		
slurry mixer	5895.6		310.3				
screen printing	396	132	66				
drying	1500	300	300	300	8		
slurry mixer	5895.6		310.3				
screen printing	396	132	66				
drying	1500	300	300	300	8		
quality control							
co-firing	204.1	31.4	15.7				
quality control							
cutting	500	400	45				
Interconnect Production Line	steel	aluminium	copper	Aluminum silicate	rubber	Ti	ceramic
stamping	10800	3600	1800		1800		
cleaning	5895.6		310.3				
arc-PVD	480	240	120			120	120
quality control							
Glass Seal Production Line	steel	aluminium	copper	Aluminum silicate	rubber	Ti	ceramic
injection molding	24	8	4				
annealing furnace	204.1	31.4	15.7				
SOEC assembly Line	steel	aluminium	copper	Aluminum silicate	rubber	Ti	ceramic
feeding interconnect							
feeding interconnect							
feeding MEA							
feeding MEA							
pressing	1750	375	125				
quality control							
UV curing	180.0	60.0	30.0	30.0	300	5.152	16

Materials to be discussed	**EU annual production 2030(estimated by market size) unit:kg**				rub
activated carbon 2022			**4GW**		
2023			**9.2GW**		
2024			**13.5GW**		
2025			**18.1GW**		
2026			**19.3GW**	300	8
2027			**19.3GW**		
2028			**19.3GW**		
2029			**19.3GW**		
2030			**19.3GW**		
drying	1500	300	300	300	8
slurry mixer	5895.6		310.3		
screen printing	396	132	66		
drying	1500	300	300	300	8
slurry mixer	5895.6		310.3		
screen printing	396	132	66		
drying	1500	300	300	300	8
slurry mixer	5895.6		310.3		
screen printing	396	132	66		
drying	1500	300	300	300	8
quality control					
co-firing	204.1	31.4	15.7		
quality control					
cutting	500	400	45		
Interconnect Production Line	steel	aluminium	copper	Aluminum silicate	rub
stamping	10800	3600	1800		180
cleaning	5895.6		310.3		
arc-PVD	480	240	120		
quality control					
Glass Seal Production Line	steel	aluminium	copper	Aluminum silicate	rub
injection molding	24	8	4		
annealing furnace	204.1	31.4	15.7		
SOEC assembly Line	steel	aluminium	copper	Aluminum silicate	rub
feeding interconnect					
feeding interconnect					
feeding MEA					
feeding MEA					
pressing	1750	375	125		
quality control					
UV curing	180.0	60.0	30.0	30.0	30

Materials to be discussed	**EU annual production 2030(estimated by market size) unit:kg**			
activated carbon 2022			**4GW**	
2023			**9.2GW**	
2024			**13.5GW**	
2025			**18.1GW**	
2026			**19.3GW**	300
2027			**19.3GW**	
2028			**19.3GW**	
2029			**19.3GW**	
2030			**19.3GW**	

	Europe			
2021	**3.5**	2.9	**1.1**	0.5
2022	**4**	**7.6**	**1.6**	0.5
2023	**9.2**	**9.1**	**1.6**	1.5
2024	**13.5**	**9.1**	**2.1**	1.5
2025	**18.1**	**12.6**	**2.1**	2.5
2026	**19.3**	**12.6**	**2.1**	2.5
2027	**19.3**	**22.6**	**2.1**	2.5
2028	**19.3**	**22.6**	**2.1**	2.5
2029	**19.3**	**22.6**	**2.1**	2.5
2030	19.3	22.6	2.1	2.5